nature cell biology

Lysosomal positioning coordinates cellular nutrient responses

Viktor I. Korolchuk[1,5], Shinji Saiki[1,5], Maike Lichtenberg[1,6], Farah H. Siddiqi[1,6], Esteban A. Roberts[2], Sara Imarisio[1,3], Luca Jahreiss[1], Sovan Sarkar[1], Marie Futter[1], Fiona M. Menzies[1], Cahir J. O'Kane[3], Vojo Deretic[2,4] and David C. Rubinsztein[1,7]

mTOR (mammalian target of rapamycin) signalling and macroautophagy (henceforth autophagy) regulate numerous pathological and physiological processes, including cellular responses to altered nutrient levels. However, the mechanisms regulating mTOR and autophagy remain incompletely understood. Lysosomes are dynamic intracellular organelles[1,2] intimately involved both in the activation of mTOR complex 1 (mTORC1) signalling and in degrading autophagic substrates[3–8]. Here we report that lysosomal positioning coordinates anabolic and catabolic responses with changes in nutrient availability by orchestrating early plasma-membrane signalling events, mTORC1 signalling and autophagy. Activation of mTORC1 by nutrients correlates with its presence on peripheral lysosomes that are physically close to the upstream signalling modules, whereas starvation causes perinuclear clustering of lysosomes, driven by changes in intracellular pH. Lysosomal positioning regulates mTORC1 signalling, which in turn influences autophagosome formation. Lysosome positioning also influences autophagosome–lysosome fusion rates, and thus controls autophagic flux by acting at both the initiation and termination stages of the process. Our findings provide a physiological role for the dynamic state of lysosomal positioning in cells as a coordinator of mTORC1 signalling with autophagic flux.

The serine/threonine kinase mTOR exists in two independent complexes. mTORC1, which contains mTOR and several regulatory subunits including raptor, controls cell metabolism, whereas mTORC2, a rictor-containing complex, modulates actin cytoskeleton dynamics[9]. At least two independent signalling events regulate mTOR activity in response to nutrient availability. One signal is initiated from growth-factor receptors that activate mTOR through the tuberous sclerosis complex (TSC1/2) and the Ras-family GTP-binding protein Ras homologue enriched in brain (Rheb). This occurs through different upstream pathways, including phosphatidylinositol-3-OH kinase (PI(3)K) and protein kinase B (PKB/Akt; refs 9–12). The mechanisms by which amino acids regulate mTOR activity are less well understood, but Rag GTPases and the Ragulator complex can mediate this response by enhancing the association of mTORC1 with the late endosomal/lysosomal compartment by bringing mTORC1 close to its activator Rheb (refs 3,4,13). mTORC1 activation stimulates protein synthesis through its phosphorylation substrates p70-S6 kinase (S6K) and eukaryotic translation initiation factor 4E-binding protein[10–12]. Conversely, starvation inactivates mTORC1, thereby inhibiting anabolic processes and liberating nutrient reserves by activating autophagy. In autophagy, cytoplasmic proteins, protein complexes and organelles are engulfed by double-membrane vesicles called autophagosomes, which are transported along microtubules towards their minus-ends and ultimately fuse with lysosomes, where their contents are degraded[5,6,8]. Thus, lysosomes are intimately involved in nutrient responses, as they are a site for mTORC1 activation and a sink for autophagy.

Nutrient deprivation has been reported to release mTOR from lysosomes, whereas amino-acid replenishment restores lysosomal localization of mTOR and its activity[3,4]. We extended these observations using three different starvation protocols (see Methods). Complete nutrient deprivation, as described previously[3,4], decreased co-localization between mTOR and the late endosomal/lysosomal markers lysosome-associated membrane protein 1 (LAMP1) or LAMP2, and inhibited mTOR activity, as assayed by the phosphorylation status of S6K at an mTOR-specific phosphorylation site (Supplementary Fig. S1a–c, data not shown). However, milder (but more physiological) starvation protocols enabled retention of mTOR on lysosomes without preventing a loss of mTOR activity (Fig. 1a,b and

[1]Department of Medical Genetics, Cambridge Institute for Medical Genetics, Wellcome Trust/MRC Building, Hills Road, Cambridge, CB2 0XY, UK. [2]Department of Molecular Genetics and Microbiology, University of New Mexico School of Medicine, Albuquerque, New Mexico, 87131, USA. [3]Department of Genetics, University of Cambridge, Cambridge, CB2 3EH, UK. [4]Department of Cell Biology and Physiology, University of New Mexico School of Medicine, Albuquerque, New Mexico, 87131, USA. [5]Joint first authors. [6]These authors contributed equally to this work.
[7]Correspondence should be addressed to D.C.R. (e-mail: dcr1000@cam.ac.uk)

Received 7 May 2010; accepted 7 January 2011; published online 13 March 2011; DOI: 10.1038/ncb2204

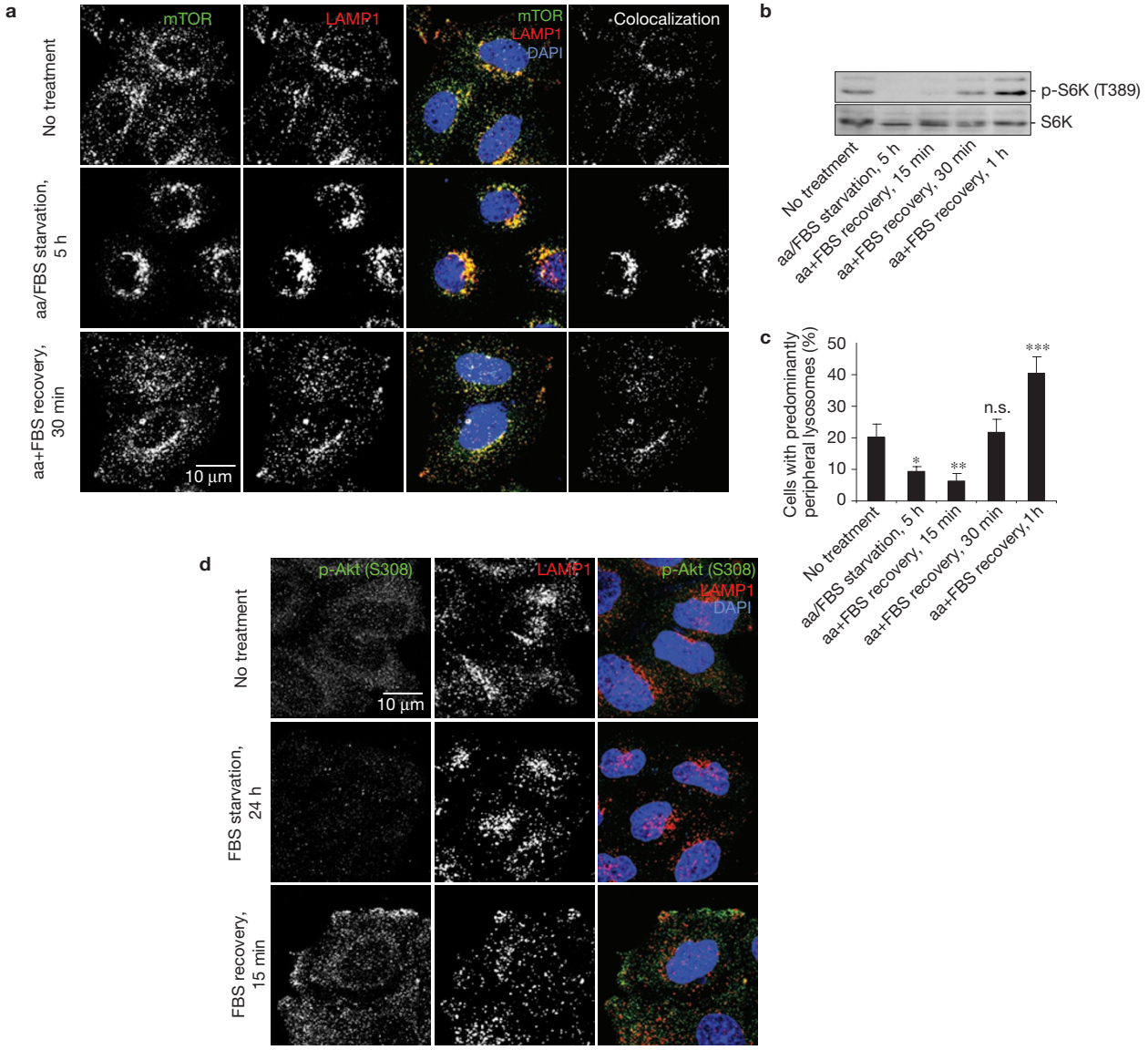

Figure 1 Changes in mTORC1 signalling in response to starvation correlate with lysosomal positioning. (**a**–**c**) HeLa cells were either left untreated, amino-acid (aa)/FBS starved for 5 h, or starved and then recovered in amino-acid/FBS-containing medium, then immunostained, or immunoblotted using antibodies as shown. Co-localization panels show an overlap between mTOR and LAMP1 signals. Note that changes in the positioning of lysosomal mTOR (quantified as the percentage of cells with predominantly peripheral localization of LAMP1-positive vesicles; **a**,**c**) correlate with mTORC1 activity (levels of phosphorylated S6K relative to the total S6K; **b**). (**d**) Visualization of Akt activated in response to recovery after serum starvation. After nutrient recovery, LAMP1-positive vesicles localize to peripheral regions with higher concentrations of phospho-Akt. DAPI, 4,6−diamidino−2−phenylindole. For all panels, values are means ± s.e.m. of three independent experiments carried out in triplicate. $^{*}P < 0.05$, $^{**}P < 0.01$, $^{***}P < 0.005$ Student's *t*-test; other comparisons are not significant (n.s.). Representative maximum-intensity projections of serial confocal optical sections are shown. Uncropped images of blots are shown in Supplementary Fig. S7.

Supplementary Fig. S1d–i). However, the intracellular distribution of lysosomes and lysosome-associated mTOR correlated with nutritional status and mTOR activity. All three starvation protocols increased the proportion of cells with predominantly perinuclear lysosomes, whereas on recovery (replenishment of amino acids either alone or together with serum) mTOR activity restoration was paralleled by the increased localization of LAMP1- and mTOR-positive vesicles at the cell periphery, including plasma-membrane projections, such as lamellipodia (Fig. 1a–c and Supplementary Fig. S1a–l). As previously described[3,4], mTORC1, rather than mTORC2, associates with lysosomes, because LAMP1-positive vesicles co-localized with the mTORC1 complex-specific subunit raptor, but not with mTORC2-specific rictor (Supplementary Fig. S2a,b).

We investigated if the correlation between mTORC1 activity and lysosomal positioning is an epiphenomenon, or if they are causally linked. First, we tested whether changes in the localization of LAMP1-positive vesicles could be a consequence of altered mTOR activity. However, neither inhibition of mTOR signalling by *raptor* or *rictor* short interfering RNA (siRNA) knockdown or with its specific inhibitor rapamycin, nor upregulation of mTORC1 activity by overexpression of mTOR, raptor or Rheb, affected the positioning of LAMP1-positive vesicles (Supplementary

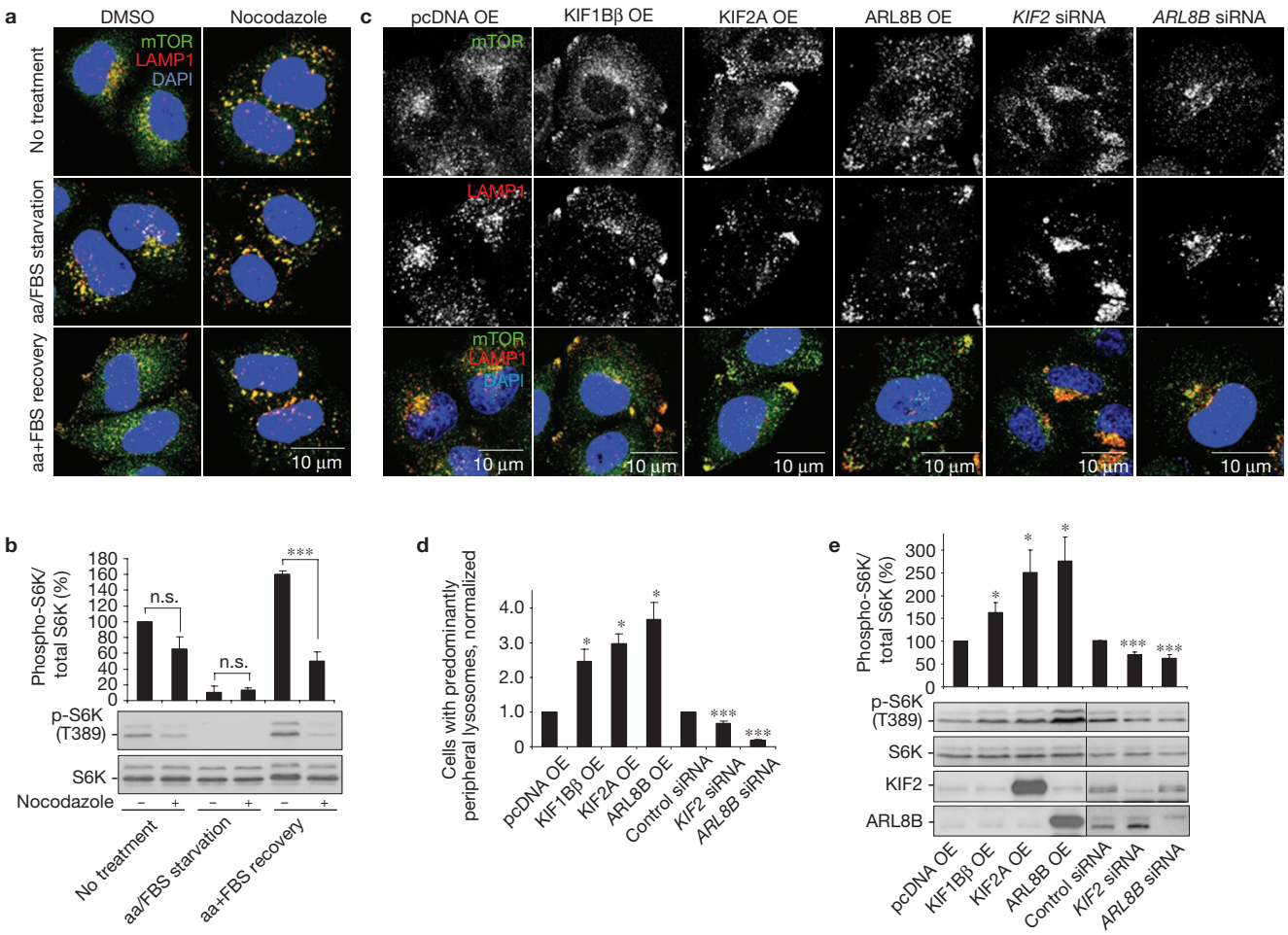

Figure 2 Factors changing lysosomal positioning also affect mTORC1 signalling. (**a**,**b**) Nocodazole flattens the differences in lysosomal mTOR localization and dampens mTORC1 signalling in response to changes in nutrient availability. Cells were treated as in Fig. 1a followed by incubation with dimethylsulphoxide (vehicle) or with nocodazole during the last 2 h before fixation/lysis. Samples were analysed by immunofluorescence (**a**) or immunoblotting (**b**). Quantification of phopho-S6K levels is shown in (**b**). (**c**–**e**) Changes in lysosomal positioning induced by kinesin- or small GTPase-family members (**c**,**d**) correlate with changes in mTORC1 activity (**e**). HeLa cells were transfected with overexpression constructs (OE) or with siRNA as shown, followed by immunofluorescence (**c**,**d**) or by immunoblotting (**e**) analyses. Values are means ± s.e.m. of three independent experiments carried out in triplicate. All comparisons are with the control within each treatment condition, $^{*}P < 0.05$, $^{***}P < 0.005$ Student's *t*-test; n.s. not significant. Uncropped images of blots are shown in Supplementary Fig. S7.

Fig. S2a–k). Similarly, lysosomal positioning was independent of Akt activity upstream of mTORC1 (Supplementary Fig. S2l–t). Therefore, we considered an alternative possibility that lysosomal positioning influenced mTORC1 activity, because the peripheral localization of lysosomal mTORC1 would bring it closer to upstream signalling molecules at the cell membrane, such as the active form of Akt, of which a major pool was detected close to the plasma membrane during the recovery phase (it is inactive during starvation; Fig. 1d; refs 14,15).

Accordingly, we investigated whether factors that alter lysosomal positioning, independent of changes in nutrient availability, affected mTORC1 activity. Short-term treatment with the microtubule-depolymerizing drug nocodazole dispersed lysosomes uniformly in the cell and obliterated any differences in lysosomal positioning seen during our starvation–recovery treatments (Fig. 2a). Nocodazole tended to suppress mTORC1 activity under basal conditions in full tissue-culture medium and prevented the full recovery of mTORC1 signalling on restoration of nutrients after starvation (Fig. 2b).

We tested our hypothesis using more specific tools by overexpressing two kinesin superfamily members, KIF1Bβ and KIF2, which redistribute lysosomes to the cell periphery[16,17]. The kinesin-induced increase in the peripheral localization of LAMP1- and mTOR-positive compartments correlated with increased mTORC1 activity (Fig. 2c–e). The small GTPase ADP-ribosylation factor-like 8B (ARL8B, also called Gie2) localizes to lysosomes and also distributes them to the periphery[18–20]. We confirmed these data and found that overexpression of ARL8B, similarly to the kinesins, increased localization of lysosomal mTORC1 at the cell periphery and enhanced its activity (Fig. 2c–e and Supplementary Fig. S3a). We also tested the converse situation by knocking down KIF2 and ARL8B and found that it resulted in clustering of lysosomes around the microtubule-organizing centre (MTOC), which correlated with reduced mTORC1 activity (Fig. 2c–e). Short-term nocodazole treatment obliterated any differences in lysosomal localization caused by ARL8B, and also flattened any differential effects of ARL8B knockdown or overexpression (Supplementary Fig. S3b). Thus, the effects of ARL8B on mTORC1 activity are unlikely to be due

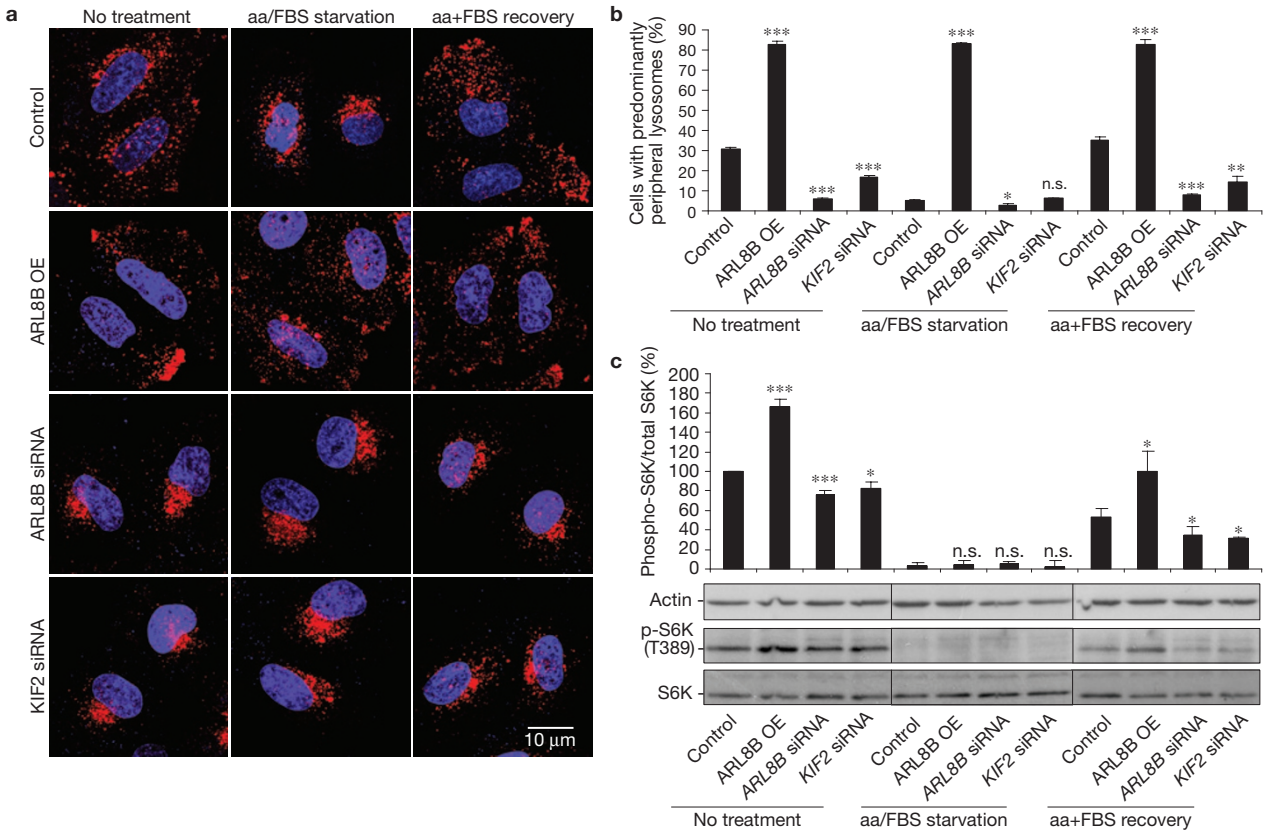

Figure 3 Lysosomal positioning regulates recovery of mTOR signalling after starvation. (**a**–**c**) HeLa cells transfected with *ARL8B* or *KIF2* siRNA, or with ARL8B overexpression construct (non-targeting siRNA and empty pcDNA vector used as transfection controls), were either left untreated, serum/amino-acid starved for 5 h, or starved and then recovered in amino-acid- and FBS-containing medium for 30 min. Cells were immunostained using LAMP1 antibody (**a**) and the percentage of cells with predominantly peripheral localization of LAMP1-positive vesicles was quantified (**b**) or subjected to immunoblotting (**c**) using antibodies as shown. Quantification of phospho-S6K levels relative to the total S6K is shown in **c**. Values are means ± s.e.m. of three independent experiments carried out in triplicate. All comparisons are with the control within each treatment condition, $^{*}P < 0.05$, $^{**}P < 0.01$, $^{***}P < 0.005$ Student's *t*-test; n.s. not significant. Uncropped images of blots are shown in Supplementary Fig. S7.

to a direct interaction of ARL8B with mTORC1, but are microtubule dependent and correlate with lysosomal localization, consistent with mTORC1 activity being regulated by lysosomal positioning.

Forcing lysosomes to the cell periphery by ARL8B overexpression, or inducing their perinuclear clustering by ARL8B or KIF2 knockdown, prevented the changes in lysosomal distribution that normally occur during starvation–recovery phases (Fig. 3a,b). This enabled us to test whether appropriate lysosomal positioning is required for the changes in mTORC1 signalling during starvation–recovery. During starvation, no mTORC1 activity was detected (assessed by S6K phosphorylation), even when lysosomes remained peripheral owing to ARL8B overexpression, indicating that peripheral localization of lysosomes and of lysosomal mTOR is not sufficient for mTORC1 signalling in the absence of upstream signalling induced by nutrients (Fig. 3a–c). However, the predominantly peripheral lysosomal localization mediated by ARL8B overexpression enhanced the induction of mTORC1 signalling on addition of nutrients after starvation, whereas preventing lysosomal spreading by ARL8B or KIF2 knockdown reduced the restoration of mTOR signalling in the recovery period (Fig. 3a–c). Therefore, lysosomal distribution seems to modulate the intensity of mTORC1 signalling response to nutrients.

To investigate mechanisms responsible for changes in lysosomal localization in response to nutrients, we tested whether our starvation–recovery protocols affected intracellular pH (pH_i), which controls lysosomal positioning[1]. All three starvation protocols increased pH_i from ~7.1 to ~7.7, returning to basal levels after nutrient restoration (Fig. 4a). Such pH_i alterations were sufficient to affect lysosomal positioning and mTORC1 activity in full tissue-culture medium (Fig. 4b–d). Importantly, changing lysosomal positioning by manipulating ARL8B or KIF2 levels did not affect pH_i (Fig. 4e). These results indicate that nutrient levels control pH_i, which changes lysosomal localization, thus affecting mTOR signalling.

We speculated that nutrients and pH_i may influence lysosomal movement by affecting binding of proteins such as KIF2 or ARL8B to lysosomes or microtubules. Both nutrient deprivation and increased pH_i reduced the levels of these proteins in lysosomal fractions, whereas restoration of nutrients or basal pH_i fully or partially reversed this phenotype (Fig. 4f,g). However, starvation and high pH_i do not seem to decrease the ability of KIF2 and ARL8B to move lysosomes by reducing their binding to polymerized microtubules (Fig. 4h,i). Thus, nutrients may stimulate lysosomal redistribution to the cell periphery by maintaining lower pH_i, which favours recruitment to lysosomes of proteins that control their intracellular positioning, whereas starvation increases pH_i and displaces these proteins from lysosomes.

By influencing mTORC1 activity, lysosomal positioning would be anticipated to regulate autophagosome formation. Perinuclear

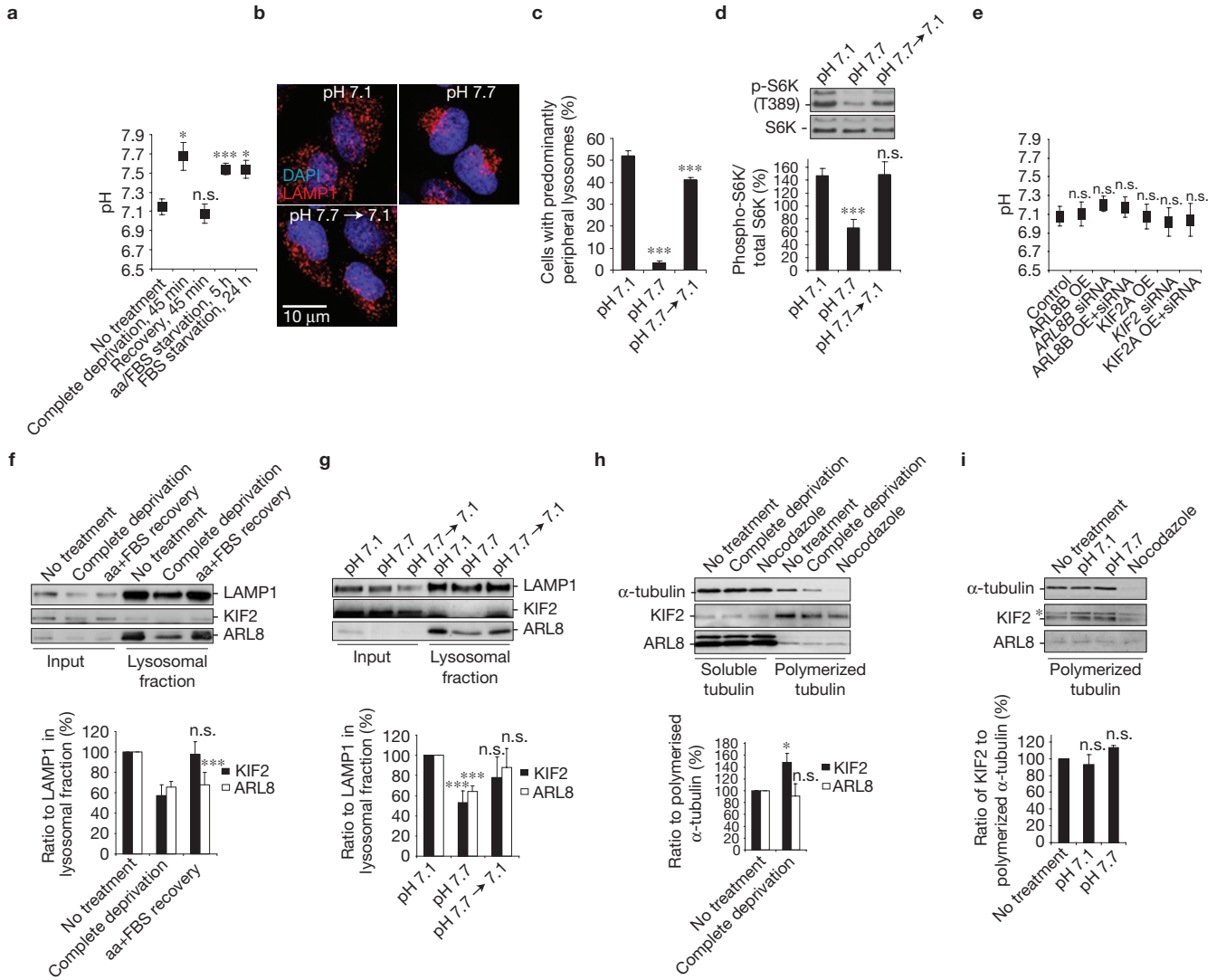

Figure 4 Nutrients control lysosomal positioning by modulating pH_i and lysosomal levels of KIF2 and ARL8B. (**a**) Starvation increases pH_i in HeLa cells allowed to starve using three different protocols (see Methods) with or without subsequent recovery. (**b**–**d**) Changing pH_i from 7.1 to 7.7 is sufficient to affect localization of lysosomes and mTORC1 activity. pH_i was titrated in full tissue-culture medium containing nigericin, which enables changes in pH_i to be forced by altering pH in the medium, followed by immunostaining (**b**,**c**) or western blotting (**d**) using antibodies as shown. (**e**) Changes in lysosomal localization have no effect on pH_i. ARL8B and KIF2 were overexpressed or knocked down in HeLa cells followed by pH_i measurement. (**f**,**g**) Nutrients and pH_i affect levels of ARL8 and KIF2 in lysosomal fractions. Protein levels and their quantification in total cellular lysates or in isolated lysosomal fractions from HeLa cells subjected to 1 h nutrient deprivation–recovery (**f**) or to 1 h changes of pH_i in full tissue-culture medium containing nigericin (**g**) are shown. (**h**,**i**) Effect of nutrients and pH_i on binding of ARL8 and KIF2 to polymerized microtubules. HeLa cells treated as in (**f**) and (**g**), followed by isolation of polymerized microtubule fraction and western blotting. The asterisk indicates a nonspecific band. For all panels values are means ± s.e.m. of three independent experiments carried out in triplicate. All comparisons are with the control within each treatment condition, $^{*}P < 0.05$, $^{**}P < 0.01$, $^{***}P < 0.005$ Student's t-test; n.s. not significant. Uncropped images of blots are shown in Supplementary Fig. S7.

positioning of lysosomes should also favour autophagosome–lysosome fusion by placing more lysosomes in the travel path of autophagosomes that form randomly in cells and move along microtubules towards the MTOC (ref. 5). Thus, lysosomal positioning may coordinate autophagic flux at both the initiation and termination stages (Fig. 5a). This would be consistent with observations that starvation, while increasing autolysosome formation (detected as an increase in the proportion of green fluorescent protein (GFP)-quenched, monomeric red fluorescent protein (mRFP)-only microtubule-associated protein 1 light chain 3 (LC3)-positive dots in cells stably expressing mRFP–GFP tandem fluorescent-tagged LC3 (tfLC3; ref. 21)), can, in some cells, reduce the steady-state numbers of autophagosomes (which correlate with the levels of the lipidated, autophagosome-associated form of LC3; LC3-II; ref. 22), indicating that starvation is simultaneously increasing the rates of autophagosome/LC3-II formation and degradation (Fig. 5b and Supplementary Fig. S4a–c).

Accordingly, we investigated whether autophagic flux is affected by factors that modulate lysosomal distribution, focusing on ARL8B, which had the strongest effect on lysosomal positioning and mTORC1 activity. We measured steady-state autophagosome/LC3-II

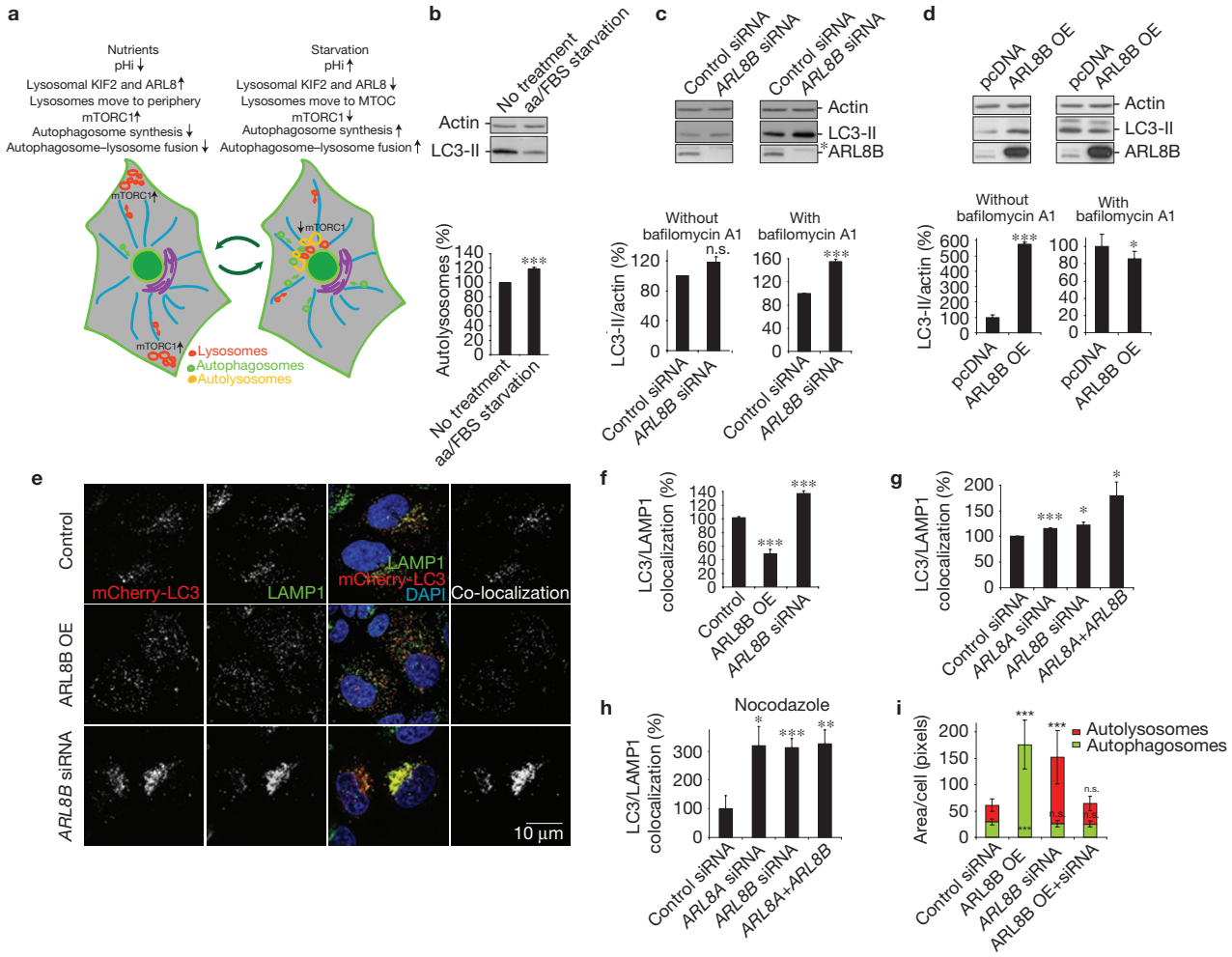

Figure 5 Lysosomal positioning modulates autophagy. (**a**) Diagram illustrating how lysosomal positioning coordinates mTOR signalling and autophagy. Peripheral lysosomal localization (nutrient induced) increases mTOR activity (blocking autophagosome synthesis) and reduces autophagosome–lysosome fusion. Starvation-induced lysosomal clustering reduces mTOR activity (activating autophagosome synthesis) and facilitates autophagosome–lysosome fusion. (**b**) Serum and amino-acid starvation of HeLa cells for 5 h reduces LC3-II levels (above), but increases autolysosome numbers detected using tfLC3 (below). With tfLC3, GFP- and RFP-positive puncta represent autophagosomes before lysosomal fusion, whereas RFP-positive/GFP-negative puncta represent autolysosomes—GFP is more rapidly quenched by low lysosomal pH (see Methods). Increased autolysosomes indicate enhanced starvation-induced flux of LC3 to lysosomes. (**c**) ARL8B knockdown increases autophagosomal synthesis. siRNA-transfected HeLa cells were incubated for 48 h, then left untreated or incubated with bafilomycin A1. LC3-II levels versus actin were quantified (bottom graphs). Asterisk: nonspecific band. (**d**) ARL8B overexpression inhibits autophagosome synthesis and degradation. HeLa cells overexpressing ARL8B or empty vector were analysed as in (**c**). (**e**) HeLa cells were co-transfected with either ARL8B overexpression construct or siRNA (non-targeting siRNA and empty peGFP vector were transfection controls) together with mCherry–LC3 for 48 h. After fixation, cells were stained for endogenous LAMP1 and DNA (DAPI). Representative maximum-intensity projections of serial confocal optical sections are shown. Co-localization panels show overlapping mCherry–LC3 and LAMP1 signals. (**f**–**h**) Quantification of autophagosome–lysosome fusion in HeLa cells. Percentages of autolysosomes (positive for both mCherry–LC3 and LAMP1) to autophagosomes (positive for mCherry–LC3 and negative for LAMP1) were quantified. In (**h**), we analysed cells treated for 2 h with nocodazole before fixation, which dispersed the perinuclear lysosomal cluster (see Fig. 2a). (**i**) Autophagosomal and autolysosomal numbers in tfLC3-expressing cells after ARL8B overexpression and knockdown (Supplementary Fig. S5o shows representative cells.). In (**f**–**i**) we analysed 20 cells per group in three independent experiments. Values are means ± s.e.m of three independent experiments carried out in triplicate. $^{*}P < 0.05$, $^{**}P < 0.01$, $^{***}P < 0.005$ Student's t-test; other comparisons not significant (n.s.). Uncropped images of blots are shown in Supplementary Fig. S7.

levels as well as autophagosome formation (levels of LC3-II in the presence of lysosomal inhibitor bafilomycin A1 that blocks its degradation)[22]. In line with our prediction (Fig. 5a), ARL8B knockdown increased autophagosome formation (LC3-II levels in the presence of bafilomycin A1) (Fig. 5c), consistent with the decreased mTOR activity (Fig. 2e). ARL8B knockdown in nutrient starvation conditions, when mTOR activity is suppressed, had no significant effect on autophagosome formation (Supplementary Fig. S4d). ARL8A, a close homologue of ARL8B, phenocopies ARL8B and the two proteins have additive effects on autophagy (Supplementary Fig. S4e,f). These ARL8 effects were confirmed using different sets of SMARTpool siRNA as well as individual siRNA oligonucleotides (Supplementary Fig. S4e–j). Similarly to ARL8A/B, knockdown of KIF2, which increased lysosomal perinuclear localization and reduced

mTORC1 activity (Fig. 2c–e), also increased autophagosome synthesis (Supplementary Fig. S4k–n).

Lysosomal scattering induced by ARL8B overexpression increased steady-state LC3-II levels and numbers of autophagic vesicles. However, in the presence of bafilomycin A1, LC3-II levels were either unaffected or even reduced (Fig. 5d and Supplementary Fig. S5a–e). Thus, ARL8B may reduce autophagosome formation (LC3-II in the presence of bafilomycin A1), as well as autophagosome–lysosome fusion (increased LC3-II in normal medium). KIF2A overexpression mimicked this effect on LC3-II levels, although its effect was less pronounced (Supplementary Fig. S5a–e). We could rescue the effects of ARL8B and KIF2A overexpression by a simultaneous knockdown of the relevant proteins demonstrating siRNA specificity (Supplementary Fig. S5a–e). As previously seen for ARL8A knockdown, its overexpression phenocopied the effect of ARL8B overexpression on LC3-II levels (Supplementary Fig. S5f).

To further test that lysosomal positioning could influence autophagosome–lysosome fusion, we measured the effect of ARL8B on the proportion of autophagosomes (marked with mCherry–LC3) that co-localizes with lysosomes (marked with anti-LAMP1 antibody or with lgp120–eGFP, a lysosomal membrane glycoprotein with a relative molecular mass (M_r) of 120K fused to enhanced green fluorescent protein). As predicted (Fig. 5a), overexpression of ARL8B decreased autophagosome–lysosome co-localization (Fig. 5e,f and Supplementary Fig. S5g,h). This autophagosome–lysosome fusion defect was not due to decreased lysosome numbers, as ARL8B overexpression did not change the expression of LAMP1, LAMP2 or mature cathepsin D (Supplementary Fig. S5i). The effect of ARL8B overexpression on autophagosome–lysosome fusion is also not due to increased mTOR activity and decreased autophagosome synthesis. First, ARL8B overexpression increased total autophagosome numbers despite decreasing autophagosome formation (Fig. 5d), indicative of a block at the fusion step. Second, ARL8B overexpression resulted in an increase in autophagosome/LC3-II levels, even when mTORC1 activity was blocked by rapamycin (Supplementary Fig. S5j). Indeed, the ability of rapamycin to reduce the accumulation of mutant huntingtin, an autophagy substrate, was blocked by ARL8B overexpression (Supplementary Fig. S5k). Finally, ARL8B inhibited autophagosome–lysosome fusion in a kinesin- and microtubule-dependent manner (Supplementary Fig. S5l–n).

Conversely, knockdown of ARL8B enhanced autophagosome–lysosome co-localization (Fig. 5e,f), whereas simultaneous knockdown of ARL8B and ARL8A additively enhanced autophagosome–lysosome fusion (Fig. 5g). This reflects increased autophagosome–lysosome fusion and not simply increased proximity in a tight perinuclear cluster, because increased co-localization was also observed after the lysosomal cluster was scattered throughout the cytoplasm by subsequent nocodazole treatment (Fig. 5h). The effects of ARL8B on autophagosome–lysosome fusion were also confirmed in tfLC3-expressing cells (Fig. 5i and Supplementary Fig. S5o).

To test the potential physiological and clinical relevance of our results we investigated the effects of ARL8 and KIF2 overexpression and knockdown on autophagic flux using diverse autophagic substrates. These include mutant forms of huntingtin associated with Huntington's disease (eGFP–httQ74; ref. 23), mutant A53T α-synuclein that causes some familial forms of Parkinson's disease (eGFP–A53T; ref. 24) and *Mycobacterium tuberculosis* var. *bovis Bacillus Calmette-Guérin* (BCG), which is related to the tuberculosis-causing mycobacterium[25,26]. ARL8 or KIF2 knockdowns had protective effects in these disease models by reducing the levels of pathogenic autophagic substrates, whereas overexpression had the opposite effects (Supplementary Fig. S6a–n). In agreement with its role in mTOR signalling and autophagy, knockdown of the *Drosophila ARL8* homologue reduced S6K phosphorylation and suppressed polyglutamine toxicity *in vivo* (Supplementary Fig. S6o,p).

In summary, lysosomes change their intracellular positioning in response to nutrient availability, thus coordinating mTORC1 activity, autophagosome synthesis and autophagosome–lysosome fusion. During starvation, mTORC1 activity is repressed, which induces autophagosome formation. Starvation increases pH_i, causing lysosomes to cluster near the MTOC, facilitating autophagosome–lysosome fusion. This may be due to a pH-dependent loss of proteins regulating anterograde lysosome movement from lysosomes. Conversely, nutrient replenishment restores basal pH_i inducing lysosomal scattering, which brings lysosomal mTORC1 to the cell periphery and stimulates its activity by increasing its coupling to the gradient of signalling molecules emanating from the plasma membrane[14,15]. The intracellular gradient of active Akt, as reported here, is consistent with previous observations, for example the localization and activation of Akt at the leading edge of chemotaxing cells[27].

Our data are consistent with multiple independent mechanisms regulating mTORC1 signalling[3,4,10,11,13]. The lysosomal association of mTORC1 is required for its activation by amino acids, but constitutive targeting of mTORC1 to lysosomes does not completely abolish its sensitivity to amino acids, indicative of other mechanisms of regulation[3]. Although lysosomal redistribution during the recovery phase after starvation may not be the initial or sole trigger for mTOR activation, lysosomal localization enables another level of control that modulates and reinforces other signalling inputs to mTOR.

Although most known autophagy-inducing signals affect autophagosome synthesis, here we show that the archetypical signal, starvation, impacts at both the synthesis and autophagosome–lysosome fusion stages, which would greatly increase the efficiency of the delivery of autophagic substrates for catabolism, compared with just increasing autophagosome synthesis. This will enhance autophagy-mediated nutrient release during starvation, facilitating the rapid availability of secondary energy sources and, therefore, cell survival. This may be an adaptation that has particular advantages in higher eukaryotic cells, where autophagosomes are generally formed at sites that are distant from lysosomes, whereas yeast autophagosomes originate close to the vacuole.

Finally, autophagy is increasingly recognized as being a central cellular process for a wide variety of human diseases, including cancer, neurodegeneration and infectious diseases. In this context, our findings may have therapeutic potential, because ARL8 proteins are GTPases and thus provide potential drug targets. For example, increased mTORC1 activity and decreased autophagy are associated with tumorigenesis, and lysosomal spreading is associated with metastasis[28]. Our data indicate that all of these phenomena may be targeted by ARL8 inhibition. Furthermore, because suppression of ARL8 activity increased the clearance of a wide range of disease-associated autophagic substrates, ARL8 inhibition may provide a tractable therapeutic target for various infectious and neurodegenerative diseases. □

METHODS

Methods and any associated references are available in the online version of the paper at http://www.nature.com/naturecellbiology/

Note: Supplementary Information is available on the Nature Cell Biology website

ACKNOWLEDGEMENTS

We thank S. Munro (Medical Research Council, Laboratory of Molecular Biology, Cambridge; ARL8 constructs and antibody), T. Katada (University of Tokyo; anti-ARL8 antibody), W. G. Kaelin (Harvard Medical School; KIF1Bβ), N. Hirokawa (University of Tokyo; KIF2), D. M. Sabatini (Massachusetts Institute of Technology; mTOR, raptor, rictor), T. Yoshimori (Osaka University; eGFP–LC3, mRFP–GFP–LC3), N. Mizushima (Tokyo Medical and Dental University; Atg5-deficient and wild-type Atg5 mouse embryonic fibroblast cell lines), W. J. Strittmatter (Duke University; Q81–eGFP), J. P. Luzio (University of Cambridge; lgp120–eGFP), A. Tolkovsky (University of Cambridge; GFP–LC3 cells), R. Tsien (University of California at San Diego; mCherry), T. Kouno (Toyama Medical and Pharmaceutical University; hLC3B) and K-L. Guan (University of California at San Diego; Rheb); B. Ravikumar, S. Luo and B. Underwood (University of Cambridge) for suggestions, M. Gratian and M. Bowen (University of Cambridge) for microscopy assistance, and the Bloomington Drosophila Stock Center. We are grateful for financial support from a Hughes Hall Research Fellowship (V.I.K. and S. Sarkar), a 2005 Pergolide Fellowship from Eli Lilly Japan (S. Saiki), the British Council Japan Association (S. Saiki), MRC studentships (M.L. and L.J.), a Daphne Jackson Trust Fellowship funded by the MRC (F.H.S.), a Heiser Foundation Postdoctoral Fellowship in Tuberculosis and Leprosy Research (E.A.R.), NIH grant AI069345, and in part NIH grants AI045148 and AI042999 (V.D.), a Wellcome Trust Senior Fellowship in Clinical Science (D.C.R.), an MRC programme grant (D.C.R., C.J.O'K.) and an EU Framework VI (EUROSCA) grant (D.C.R.).

AUTHOR CONTRIBUTIONS

All authors designed and analysed experiments. V.I.K., S. Saiki, M.L., F.H.S., E.A.R., S.I., L.J., S. Sarkar, M.F. and F.M.M. carried out experiments. V.I.K. and D.C.R. wrote the manuscript. D.C.R. supervised the project.

COMPETING FINANCIAL INTERESTS

The authors declare no competing financial interests.

Published online at http://www.nature.com/naturecellbiology
Reprints and permissions information is available online at http://npg.nature.com/reprintsandpermissions/

1. Heuser, J. Changes in lysosome shape and distribution correlated with changes in cytoplasmic pH. *J. Cell Biol.* **108,** 855–864 (1989).
2. Luzio, J. P., Pryor, P. R. & Bright, N. A. Lysosomes: fusion and function. *Nat. Rev. Mol. Cell Biol.* **8,** 622–632 (2007).
3. Sancak, Y. *et al.* Ragulator-Rag complex targets mTORC1 to the lysosomal surface and is necessary for its activation by amino acids. *Cell* **141,** 290–303 (2010).
4. Sancak, Y. *et al.* The Rag GTPases bind raptor and mediate amino acid signalling to mTORC1. *Science* **320,** 1496–1501 (2008).
5. Jahreiss, L., Menzies, F. M. & Rubinsztein, D. C. The itinerary of autophagosomes: from peripheral formation to kiss-and-run fusion with lysosomes. *Traffic* **9,** 574–587 (2008).
6. Kimura, S., Noda, T. & Yoshimori, T. Dynein-dependent movement of autophagosomes mediates efficient encounters with lysosomes. *Cell Struct. Funct.* **33,** 109–122 (2008).
7. Klionsky, D. J. Autophagy: from phenomenology to molecular understanding in less than a decade. *Nat. Rev. Mol. Cell Biol.* **8,** 931–937 (2007).
8. Ravikumar, B. *et al.* Mammalian macroautophagy at a glance. *J. Cell Sci.* **122,** 1707–1711 (2009).
9. Sengupta, S., Peterson, T. R. & Sabatini, D. M. Regulation of the mTOR complex 1 pathway by nutrients, growth factors, and stress. *Mol. Cell* **40,** 310–322 (2010).
10. Tee, A. R., Anjum, R. & Blenis, J. Inactivation of the tuberous sclerosis complex-1 and -2 gene products occurs by phosphoinositide 3-kinase/Akt-dependent and -independent phosphorylation of tuberin. *J. Biol. Chem.* **278,** 37288–37296 (2003).
11. Tee, A. R., Manning, B. D., Roux, P. P., Cantley, L. C. & Blenis, J. Tuberous sclerosis complex gene products, Tuberin and Hamartin, control mTOR signaling by acting as a GTPase-activating protein complex toward Rheb. *Curr. Biol.* **13,** 1259–1268 (2003).
12. Soulard, A. & Hall, M. N. SnapShot: mTOR signaling. *Cell* **129,** 434 (2007).
13. Kim, E., Goraksha-Hicks, P., Li, L., Neufeld, T. P. & Guan, K. L. Regulation of TORC1 by Rag GTPases in nutrient response. *Nat. Cell Biol.* **10,** 935–945 (2008).
14. Cai, S. L. *et al.* Activity of TSC2 is inhibited by AKT-mediated phosphorylation and membrane partitioning. *J. Cell Biol.* **173,** 279–289 (2006).
15. Jiang, H. & Vogt, P. K. Constitutively active Rheb induces oncogenic transformation. *Oncogene* **27,** 5729–5740 (2008).
16. Santama, N. *et al.* KIF2β, a new kinesin superfamily protein in non-neuronal cells, is associated with lysosomes and may be implicated in their centrifugal translocation. *EMBO J.* **17,** 5855–5867 (1998).
17. Matsushita, M., Tanaka, S., Nakamura, N., Inoue, H. & Kanazawa, H. A novel kinesin-like protein, KIF1Bβ3 is involved in the movement of lysosomes to the cell periphery in non-neuronal cells. *Traffic* **5,** 140–151 (2004).
18. Bagshaw, R. D., Callahan, J. W. & Mahuran, D. J. The Arf-family protein, Arl8b, is involved in the spatial distribution of lysosomes. *Biochem. Biophys. Res. Commun.* **344,** 1186–1191 (2006).
19. Hofmann, I. & Munro, S. An N-terminally acetylated Arf-like GTPase is localised to lysosomes and affects their motility. *J. Cell Sci.* **119,** 1494–1503 (2006).
20. Okai, T. *et al.* Novel small GTPase subfamily capable of associating with tubulin is required for chromosome segregation. *J. Cell Sci.* **117,** 4705–4715 (2004).
21. Kimura, S., Noda, T. & Yoshimori, T. Dissection of the autophagosome maturation process by a novel reporter protein, tandem fluorescent-tagged LC3. *Autophagy* **3,** 452–460 (2007).
22. Tanida, I., Minematsu-Ikeguchi, N., Ueno, T. & Kominami, E. Lysosomal turnover, but not a cellular level, of endogenous LC3 is a marker for autophagy. *Autophagy* **1,** 84–91 (2005).
23. Ravikumar, B., Duden, R. & Rubinsztein, D. C. Aggregate-prone proteins with polyglutamine and polyalanine expansions are degraded by autophagy. *Hum. Mol. Genet.* **11,** 1107–1117 (2002).
24. Webb, J. L., Ravikumar, B., Atkins, J., Skepper, J. N. & Rubinsztein, D. C. α-Synuclein is degraded by both autophagy and the proteasome. *J. Biol. Chem.* **278,** 25009–25013 (2003).
25. Gutierrez, M. G. *et al.* Autophagy is a defense mechanism inhibiting BCG and Mycobacterium tuberculosis survival in infected macrophages. *Cell* **119,** 753–766 (2004).
26. Singh, S. B., Davis, A. S., Taylor, G. A. & Deretic, V. Human IRGM induces autophagy to eliminate intracellular mycobacteria. *Science* **313,** 1438–1441 (2006).
27. Merlot, S. & Firtel, R. A. Leading the way: directional sensing through phosphatidylinositol 3-kinase and other signaling pathways. *J. Cell Sci.* **116,** 3471–3478 (2003).
28. Mohamed, M. M. & Sloane, B. F. Cysteine cathepsins: multifunctional enzymes in cancer. *Nat. Rev. Cancer* **6,** 764–775 (2006).

METHODS

Cell lines. Human cervical carcinoma (HeLa) cells, autophagy-related protein 5 (Atg5)-deficient ($Atg5^{-/-}$) and wild-type ($Atg5^{+/+}$) mouse embryonic fibroblast cell lines[29], normal rat kidney cells and RAW264.7 macrophages were cultured in DMEM with 4 mM L-glutamine and 10% fetal bovine serum (FBS) — full tissue-culture medium. Inducible HeLa cell lines stably expressing eGFP–A53T were established using a HeLa Tet-on line (Clontech) and cultured in DMEM supplemented with 10% FBS, 2 mM L-glutamine, 100 units ml^{-1} penicillin–streptomycin, 100 $\mu g\,ml^{-1}$ G418 (GIBCO) and 200 $\mu g\,ml^{-1}$ hygromycin B. Cells were transfected using Lipofectamine and Lipofectamine 2000 (Invitrogen) or by nucleoporation (Amaxa) according to the manufacturer's protocols. In some experiments, cells were treated for 4–16 h with 200–400 nM bafilomycin A1 or for 1–5 h with 1 μM nocodazole before collection or fixation. All chemicals were from Sigma unless indicated otherwise.

Plasmids. Huntington's disease gene exon 1 fragment with 74 polyQ repeats in peGFP-C1 (Clontech; *eGFP–httQ74*) or in pHM6 (Roche Diagnostics; *httQ74–HA*), *Q81–eGFP*, peGFP-α-synuclein^{A53T} (*eGFP*^{A53T}), haemagglutinin (*HA*)- or *eGFP*-tagged *ARL8B* wild type, *HA*- or *eGFP*-tagged *ARL8B*^{Q75L} (*ARL8B-CA*) and *HA*- or *eGFP*-tagged *ARL8A* wild type (refs 19,30–33), *KIF1Bβ* (ref. 34), *KIF2A* (ref. 30), *Myc–mTOR* (ref. 35), *Myc–Raptor* (ref. 35), *Myc–Rictor* (ref. 35), *lgp120–eGFP* (ref. 36), pcDNA3-HA/Rheb (ref. 37) and *tfLC3* (ref. 21) constructs have been described previously.

Wild-type *ARL8A–Flag*, wild-type *ARL8B–Flag* and *ARL8B*^{Q75L} (*ARL8B-CA*)*–Flag* vectors were derived by inserting *ARL8A* or *ARL8B* complementary DNA into pCMV5a containing the carboxy-terminal *Flag* tag (Sigma) using SalI and KpnI. *ARL8B* fused to cyan fluorescent protein (*CFP*) was obtained by cloning *ARL8B* cDNA into pECFP-N1 (Clontech) using XhoI and BamHI. To generate *mCherry–LC3*, the *mCherry* DNA was amplified using pRSET-B as a template using the following primers: 5′-TA CCG AGC TCG GTA CCC GCC ACC AT-3′ and 3′-G CTG TAC AAG GAA GGA TCC TGC-5′. The resulting fragment was inserted into the 5′ end of *hLC3B* in pcDNA3 (Invitrogen). All restriction endonucleases were purchased from New England BioLabs.

siRNA. ON-TARGETplus SMARTpool siRNA against human *ARL8B* (J-020294-09 or L-020294-01), mouse *ARL8B* (J-056525-09), human *ARL8A* (L-016577-01), human *KIF2A* (L-004959-00), human *raptor* (L-004107-00), human *rictor* (L-016984-00), human *Akt1* (L-003000-00), non-targeting SMARTpool siRNA (D-001810-04) and individual oligonucleotides of siRNA against human *ARL8B* (LQ-020294-01-0002) and *KIF2* (LQ-004959-00-0002) were purchased from Dharmacon. An alternative set of Stealth/siRNA duplex oligonucleotides against *ARL8B* (127338D10) and *ARL8A* (127338D09) was purchased from Invitrogen. The *ARL8B* siRNAs do not match sequences in *ARL8A* and *vice versa*. Final siRNA concentrations of 50 or 100 nM were used for silencing.

Starvation and recovery protocols. Three starvation protocols were used. Protocol 1 was complete nutrient deprivation. HeLa cells grown in wells of six-well plates were washed briefly in 2 ml of Hanks Balanced Salt Solution (Sigma H9394 or GIBCO 14025), media aspirated, and 2 ml of fresh Hanks Balanced Salt Solution was added followed by 45 min incubation at 37 °C. Protocol 2 was milder serum and amino-acid starvation. Full tissue-culture medium in six-well plates was aspirated, 2 ml of Hanks Balanced Salt Solution was added and incubated at 37 °C for 5 h. Protocol 3 was serum starvation. Cells in wells of six-well plates were washed briefly in 2 ml of serum-free DMEM (containing ×1 amino acids, Sigma D6546), media aspirated, and 2 ml of fresh serum-free DMEM was added followed by 24 h incubation at 37 °C. Recovery after starvation was achieved by addition of 2 ml DMEM with extra ×1 amino acids (MEM amino acids ×50 liquid, GIBCO 11130051, and L-glutamine, Sigma G7513) with or without 5% FBS (Sigma, F7524) at pH 7.2. For experiments in 24-well plates, volumes of the media were reduced to 0.5 ml per well.

Immunoblotting. The procedure has been described before[38]. The following primary antibodies were used in this study: anti-human ARL8 that recognizes both ARL8A and ARL8B (1:1,000; ref. 20), anti-ARL8B (ProteinTech Group, 1:1,000), anti-KIF2 (Abnova, 1:1,000), anti-GFP (Clontech, 1:2,000), anti-actin (1:2,000), anti-tubulin (1:2,000), anti-Flag (1:1,000), anti-HA (Covance, 1:1,000), anti-LC3 (Novus Biologicals, 1:2,000), anti-Atg5 (Novus Biologicals, 1:1,000), anti-S6 ribosomal protein (Cell Signaling, 1:1,000), anti-phospho-S6 ribosomal protein (Ser 235/236; Cell Signaling, 1:1,000), anti-p70 S6K (Cell Signaling, 1:1,000), anti-phospho-p70 S6K (Thr 389) (Cell Signaling, 1:1,000), anti-Bcl-2 (Cell Signaling, 1:1,000), anti-phospho-Bcl-2 (Ser 70; Cell Signaling, 1:1,000), anti-cathepsin D (Abcam, 1:1,000), anti-LAMP1 (Developmental Studies Hybridoma Bank, 1:500), anti-LAMP2 (Developmental Studies Hybridoma Bank, 1:500), anti-raptor (Origene, 1:500), anti-rictor (Bethyl Laboratories, 1:1,000), anti-Akt (Cell Signaling, 1:1,000), anti-*Drosophila* ARL8 antibody (1:1,000; ref. 19) and anti-phospho-*Drosophila* p70 S6K (Thr 398) antibody (Cell Signaling, 1:1,000). Secondary antibodies were either horse radish peroxidase (HRP) conjugated (Roche, 1:5,000) and the signal was detected by autoradiography using an enhanced chemiluminescence western blotting kit (GE Healthcare) or conjugated to IRDye for detection at 780 or 680 nm (Li-Cor Biosciences) and visualized and quantified using an Odyssey imaging system (Li-Cor Biosciences).

Immunofluorescence. The procedure for immunofluorescence, cell death and aggregate count has been described before[38]. The following primary antibodies were used in this study: anti-human ARL8 that recognizes both ARL8A and ARL8B (1:100), anti-HA antibody (Covance, 1:500), anti-Flag (1:500), anti-LAMP1, anti-LAMP2 and anti-CD63 (Developmental Studies Hybridoma Bank, 1:1,000), anti-LC3 (NanoTools, 1:500), anti-mTOR (Cell Signaling, 1:200), anti-phospho-mTOR (Ser2448) (Cell Signaling, 1:100), anti-phospho-Akt (S308) (Cell Signaling, 1:100), anti-raptor (Origene, 1:50) or anti-rictor (Bethyl Laboratories, 1:200).

Co-localization measurements. The Colocalization plugin in ImageJ (NIH) was applied to measure co-localization between two channels of confocal *z* stacks (a constant threshold for all of the images within each experiment was applied). A maximum-intensity projection was generated and the area of co-localizing pixels (including objects of three pixels and above) was quantified using the Analyse Particles plugin in ImageJ and expressed as the total area of co-localization per cell. Quantification was carried out on at least 20 cells per condition from two to four independent experiments.

To measure co-localization between mCherry–LC3 vesicles and lysosomes, cells were co-transfected with plasmid DNA and siRNA against proteins of interest together with mCherry–LC3 (and for some experiments with lgp120–eGFP). In some experiments, cells were immunostained using mouse monoclonal LAMP1 antibody. The percentage of mCherry–LC3 vesicles co-localizing with late endosomes/lysosomes (LAMP1 or lgp120–eGFP positive) to the total number of mCherry–LC3 vesicles was calculated from stacks of confocal images through the whole thickness of the cell using ImageJ (NIH) or Volocity (Improvision). All of the values were normalized to the control.

Quantification of lysosomal distribution. To score lysosomal distribution, cells were categorized into perinuclear-dominant lysosomal pattern (more than 50% of LAMP1- or lgp120–eGFP-positive vesicles localized in the perinuclear region) and peripheral-dominant pattern (more than 50% of the vesicles localized in the peripheral region), on the basis of the number of lysosomes in each region. Quantification is based on at least three independent experiments, each carried out in triplicate, and 100–200 cells were counted in each slide; the scorer was blinded to treatment. The data are expressed as a proportion of cells with predominantly (>50%) peripheral lysosomes.

Measurement and manipulation of pH_i. pH_i was determined using pH-sensitive fluorescent dye 2′7′-bis-(2-carboxyethyl)-5-(and-6)-carboxyfluorescein-acetoxymethyl (Invitrogen) as described[39]. Fluorescence was measured with Cytofluor Multiplate reader (PerSeptive Biosystems) or Multilabel reader EnVision 2103 (Perkin Elmer). Two fluorescence measurements were made at (1) an excitation wavelength (λ_{ex}) of 485 nm and an emission wavelength (λ_{em}) of 530 nm and (2) a λ_{ex} of 450 nm and a λ_{em} of 530 nm; the fluorescence ratio (1)/(2) was used to calculate pH_i. To change pH_i, cells were incubated for 50 min at 37 °C in full tissue-culture medium that contained nigericin, which enables changes in pH_i to be forced by altering the pH in the medium. When the pH of the medium was adjusted to 6.5 and 8, the pH_i changed (from 7.2 under normal conditions) to 7.1 and 7.7–7.8, respectively, as determined by the calibration curve.

Lysosome- and microtubule-isolation protocols. Lysosomes were isolated with the Lysosome Enrichment Kit for Tissue and Cultured Cells (Thermo Scientific) according to the manufacturer's instructions. Isolation of polymeric microtubules was carried out using the centrifugation method as previously described[40].

Autophagy analyses. Measuring the levels of endogenous LC3-II/actin ratios as a readout for autophagosome numbers has been previously described[41]. To quantify endogenous LC3-positive vesicles, cells were immunolabelled using anti-LC3 antibody (NanoTools). Slides were scored for a percentage of cells with more than 20 LC3-positive vesicles. All experiments were carried out

DOI: 10.1038/ncb2204

in triplicate with at least 200 cells counted per slide; the scorer was blinded to treatment.

Automated microscope counting of autolysosomes labelled with a pH-sensitive tfLC3 was carried out using a Thermo Scientific Cellomics ArrayScan VTI HCS reader and the Spot Detector Bioapplication protocol, version 3, as already described[41]. With tfLC3, GFP- (and RFP-) positive puncta represent autophagosomes before lysosomal fusion, whereas RFP-positive puncta (that lack GFP fluorescence) represent autolysosomes (as the GFP is more rapidly quenched by the low pH; ref. 21). Alternatively, total areas of GFP–RFP and RFP-only positive puncta per cell were quantified from *z* stacks of confocal images using ImageJ and the Analyse Particles plugin (a constant threshold for all of the images within each experiment was applied). At least 20 cells per condition in three independent experiments were used for quantification.

BCG colony-forming-unit assay. After transfection by nucleoporation, cells were infected with live BCG for 1 h, washed to remove extracellular mycobacteria and incubated for 2 h in full medium or Earle's Balanced Salt Solution (starvation). Macrophages were then hypotonically lysed using cold sterile water; mycobacteria were plated on Middlebrook 7H11 agar followed by incubation at 37 °C for 2–3 weeks and colony-forming-unit counting.

***Drosophila* stocks and crosses.** Examination of gross eye and pseudopupil phenotypes was carried out on progeny of the appropriate genotype, generated by crossing virgins of the genotype *y w; gmr-Htt(exon1)Q120* either with w^{1118}; *PBac[RB]ARL8* ^{e00336}/ *TM6B, Tb* (ref. 1) (stock 17846 from the Bloomington *Drosophila* stock centre) or with one of two control lines: an isogenic w^{1118} line[42], or w^{1118}; *PBac[RB]CG33523* ^{e03176} (stock 18128 from the Bloomington *Drosophila* stock centre). The latter flies were used as an extra control for genetic background, because they carry a homozygous viable insertion of the same construct in the same genetic background as the *ARL8* insertion[43]. Virgins of the isogenic w^{1118} line were crossed with males of the two *PBac[RB]* insertion lines, to generate progeny to confirm that neither insertion alone resulted in neurodegeneration when heterozygous. Note that *Drosophila Arl8* has also been designated as *Gie*[20].

Statistical analyses. Protein levels, vesicle distribution, numbers and co-localization of vesicles, aggregate formation, cell death and BCG survival were expressed as percentages from three independent experiments carried out in triplicate, and the error bars denote standard error of the mean. *P* values were determined by Student's *t*-test (Microsoft Excel) where stated or by unconditional logistical regression analysis, using the general log–linear analysis option of SYSTAT10.2 (SYSTAT Software). A paired Student's *t*-test was used to compare averages of *Drosophila* rhabdomeres.

29. Kuma, A. *et al*. The role of autophagy during the early neonatal starvation period. *Nature* **432,** 1032–1036 (2004).
30. Noda, Y., Sato-Yoshitake, R., Kondo, S., Nangaku, M. & Hirokawa, N. KIF2 is a new microtubule-based anterograde motor that transports membranous organelles distinct from those carried by kinesin heavy chain or KIF3A/B. *J. Cell Biol.* **129,** 157–167 (1995).
31. Berger, Z. *et al*. Rapamycin alleviates toxicity of different aggregate-prone proteins. *Hum. Mol. Genet.* **15,** 433–442 (2006).
32. Narain, Y., Wyttenbach, A., Rankin, J., Furlong, R. A. & Rubinsztein, D. C. A molecular investigation of true dominance in Huntington's disease. *J. Med. Genet.* **36,** 739–746 (1999).
33. Sarkar, S. *et al*. A rational mechanism for combination treatment of Huntington's disease using lithium and rapamycin. *Hum. Mol. Genet.* **17,** 170–178 (2008).
34. Schlisio, S. *et al*. The kinesin KIF1Bβ acts downstream from EglN3 to induce apoptosis and is a potential 1p36 tumor suppressor. *Genes Dev.* **22,** 884–893 (2008).
35. Sarbassov, D. D. *et al*. Rictor, a novel binding partner of mTOR, defines a rapamycin-insensitive and raptor-independent pathway that regulates the cytoskeleton. *Curr. Biol.* **14,** 1296–1302 (2004).
36. Pryor, P. R., Reimann, F., Gribble, F. M. & Luzio, J. P. Mucolipin-1 is a lysosomal membrane protein required for intracellular lactosylceramide traffic. *Traffic* **7,** 1388–1398 (2006).
37. Zhou, X. *et al*. Rheb controls misfolded protein metabolism by inhibiting aggresome formation and autophagy. *Proc. Natl Acad. Sci. USA* **106,** 8923–8928 (2009).
38. Korolchuk, V. I., Mansilla, A., Menzies, F. M. & Rubinsztein, D. C. Autophagy inhibition compromises degradation of ubiquitin-proteasome pathway substrates. *Mol. Cell* **33,** 517–527 (2009).
39. Tafani, M. *et al*. Regulation of intracellular pH mediates Bax activation in HeLa cells treated with staurosporine or tumor necrosis factor-α. *J. Biol. Chem.* **277,** 49569–49576 (2002).
40. Ong, V. *et al*. A role for altered microtubule polymer levels in vincristine resistance of childhood acute lymphoblastic leukemia xenografts. *J. Pharmacol. Exp. Ther.* **324,** 434–442 (2008).
41. Sarkar, S., Korolchuk, V., Renna, M., Winslow, A. & Rubinsztein, D. C. Methodological considerations for assessing autophagy modulators: a study with calcium phosphate precipitates. *Autophagy* **5,** 307–313 (2009).
42. Ryder, E. *et al*. The DrosDel collection: a set of P-element insertions for generating custom chromosomal aberrations in Drosophila melanogaster. *Genetics* **167,** 797–813 (2004).
43. Thibault, S. T. *et al*. A complementary transposon tool kit for Drosophila melanogaster using P and piggyBac. *Nat. Genet.* **36,** 283–287 (2004).

nature cell biology

DOI: 10.1038/ncb2204

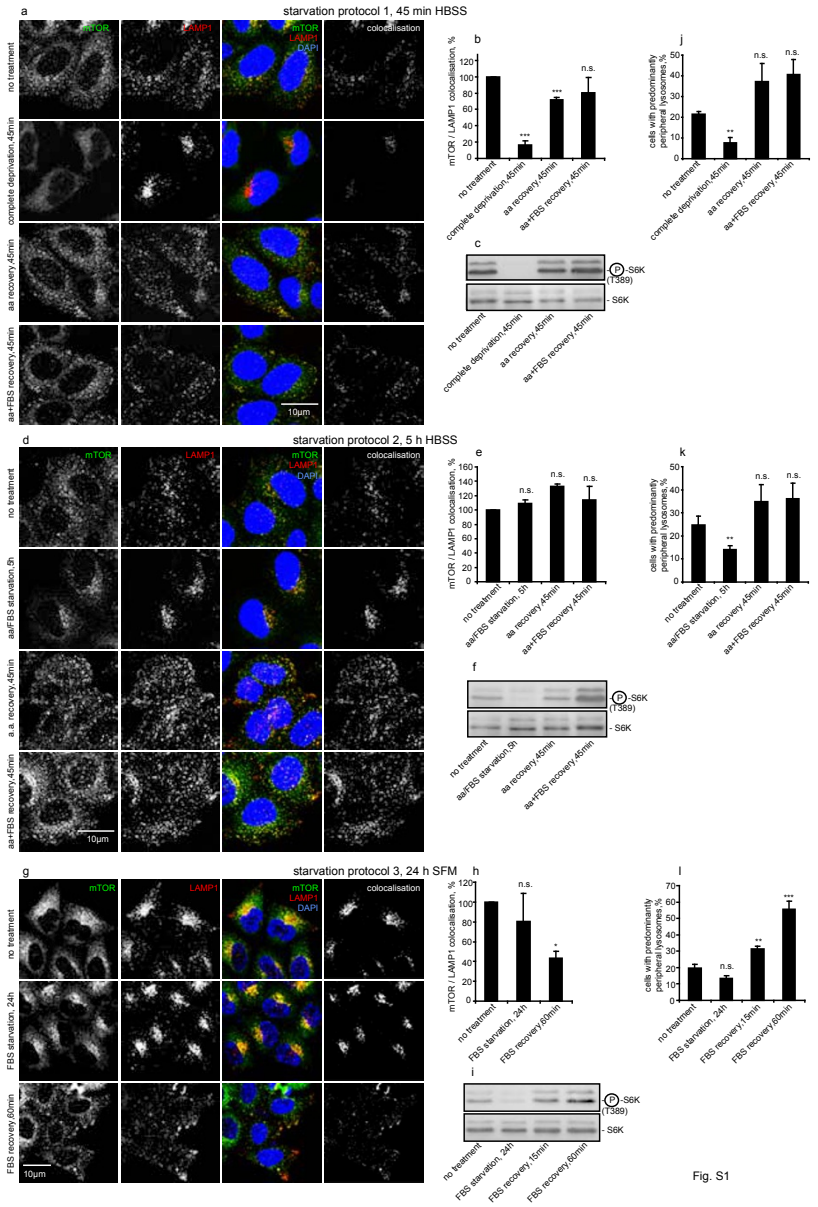

Figure S1 Three different starvation/recovery protocols produce similar changes in lysosomal positioning. (a-c) HeLa cells were left untreated, completely deprived of amino acids and serum by rinsing and then incubating in HBSS medium for 45 min, (protocol 1, see Methods) or deprived of nutrients in this way and then recovered for 45 min in DMEM supplemented with x1 amino acids or in full tissue culture medium. (a) Confocal images of immunolabelled cells (where anti-LAMP1, anti-mTOR antibodies and DAPI are used to detect endogenous proteins and nuclear DNA) and colocalisation between LAMP1 and mTOR are shown as maximum intensity projections. Note that mTOR is released from the LAMP1-positive compartment during this starvation procedure, in agreement with other studies [19, 20]. (b) Colocalisation between LAMP1 and mTOR is quantified using images of 10-20 cells from 3 independent experiments; data are expressed as normalised area of colocalisation per cell. (c) Immunoblots illustrate changes in mTOR signaling (p70-S6 kinase phosphorylation at an mTORC1-specific site compared to total p70-S6 kinase) in cells treated as in (a). (d-f) HeLa cells were left untreated, starved by replacing (without wash) the nutrient-rich medium with HBSS for 5 h (protocol 2), or starved and then recovered for 45 min in the nutrient-rich medium. The starvation procedure is the same as used to obtain the data shown in Fig.1a-c of the main text. Cells were subjected to the same analyses as in panels (a-c). Note that this starvation protocol does not lead to the release of mTOR from the LAMP1-positive compartment during this starvation procedure. (g-i) HeLa cells were left untreated, starved by incubating in serum-free DMEM for 24 h (protocol 3), or starved and then recovered in 5% FBS- supplemented DMEM, for 15 or 60 min. The starvation procedure is the same as used to obtain the data shown in Fig.1d of the main text. Cells were analysed as in panels (a-c). (j-l) The quantification of changes in lysosomal positioning (expressed as a percentage of cells with predominantly peripheral lysosomes) in cells treated according to the starvation protocol 1 (j), protocol 2 (k) and protocol 3 (l).

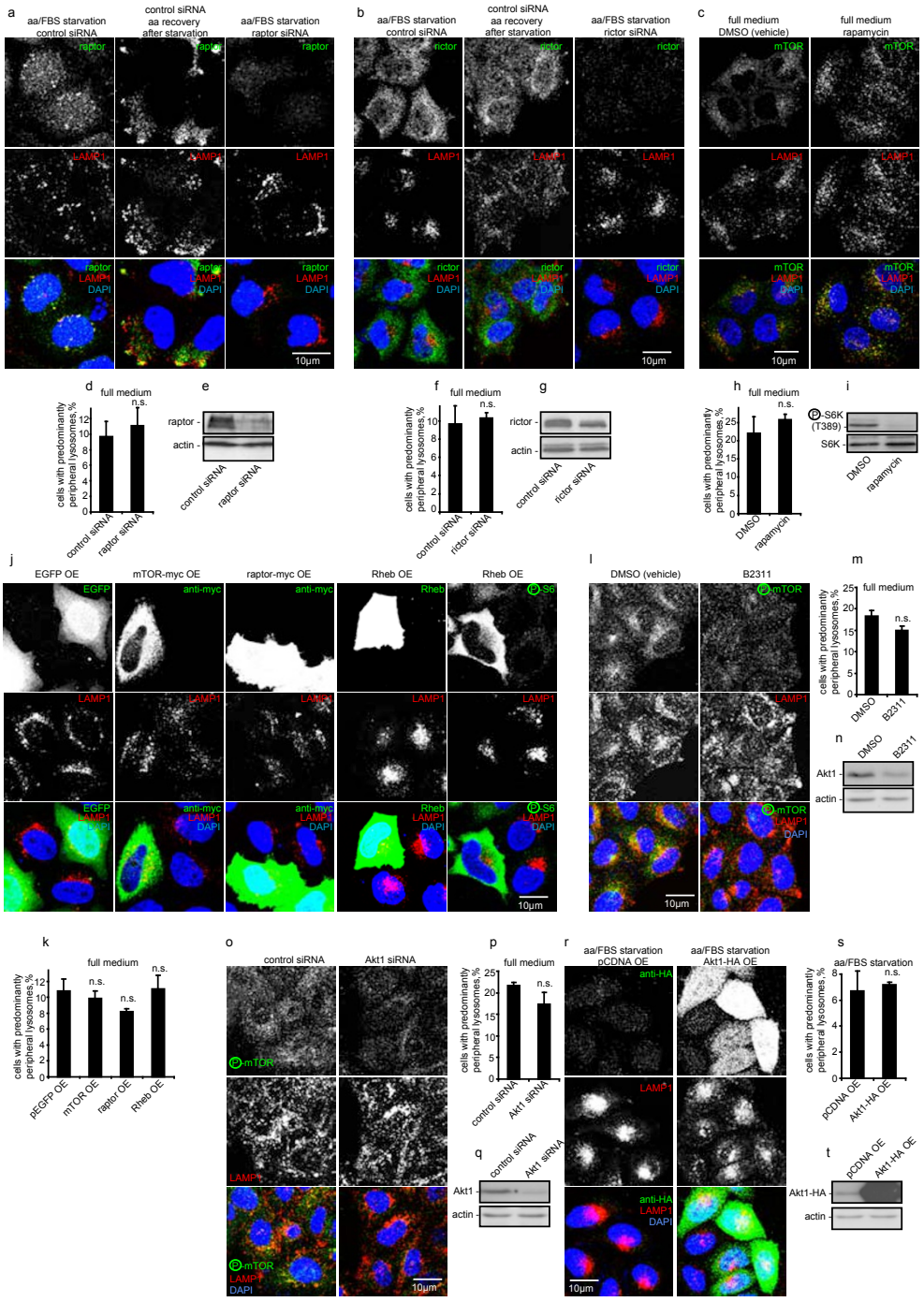

Figure S2 Akt/mTORC1 signaling does not affect intracellular lysosomal positioning. (a) Endogenous raptor (component of mTORC1 complex) partially colocalises with LAMP1-positive vesicles both in starved (starvation protocol 2, incubation in HBSS medium for 5 h) and nutrient-replete HeLa cells. (b) Endogenous rictor (a component of mTORC2 complex) does not colocalise with LAMP1-positive vesicles and its knockdown does not influence lysosomal positioning. In panels (a) and (b) knockdown of raptor and rictor by siRNA confirms specificity of antibodies used for immunofluorescence. (c) Inhibition of mTORC1 by rapamycin does not affect lysosomal positioning. Note that inactivated by rapamycin mTOR is found almost exclusively on LAMP1-positive vesicles. (d-i) siRNA-mediated knockdown of raptor and rictor (visualised by immunoblotting using antibodies against raptor and rictor) and inactivation of mTOR by rapamycin (visualised by p70-S6 kinase phosphorylation at mTORC1-specific site compared to total protein) do not affect intracellular positioning of LAMP1-positive vesicles. (j) and (k) Upregulation of mTORC1 signaling by overexpression of mTOR, raptor or Rheb does not induce distribution of lysosomes to cell periphery. Activation of mTOR by Rheb is visualised by staining against phospho-S6 protein, a p70-S6 kinase substrate downstream of mTORC1 signaling. (l-n) Inhibition of Akt1 by 10 μM 5-(2-Benzothiazolyl)-3-ethyl-2-[2-(methylphenylamino) ethenyl]-1-phenyl-1H-benzimidazolium iodide (B2311, Sigma) for 16 h does not affect lysosomal positioning. Inhibition of Akt is visualised with anti-phospho-mTOR antibody by immunofluorescence and leads to reduced levels of Akt1 as detected by western blotting. (o-q) Knockdown of Akt1 does not affect localisation of lysosomes but reduces phosphorylation of mTOR and levels of Akt1. (r-t) Overexpression of Akt1-HA does not affect lysosomal positioning in starved for 5 h cells (r) and (s) or in cells grown in complete medium (data not shown).

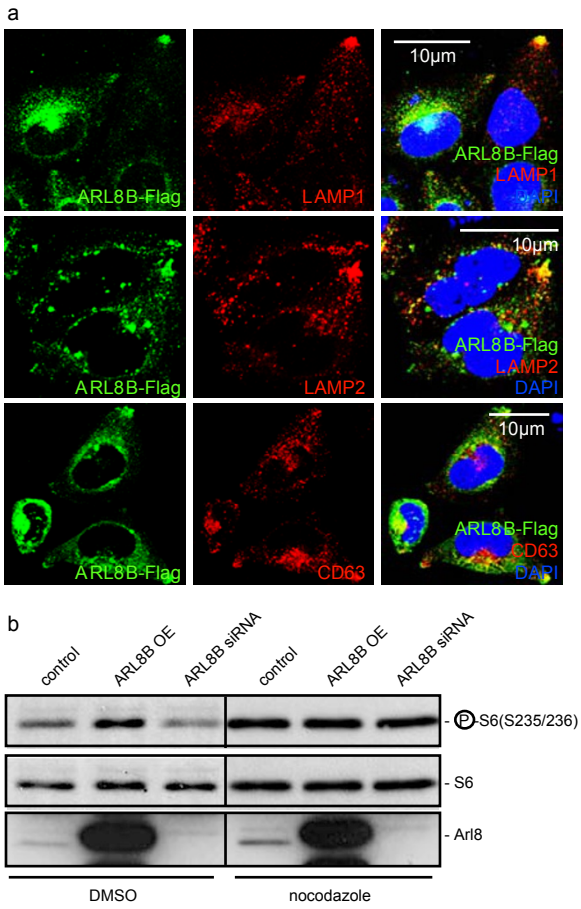

Figure S3 ARL8B colocalises with markers of late endosomes/lysosomes and induces peripheral localisation of lysosomes. (a) Overexpressed and endogenous ARL8B partially colocalises with late endosomal/lysosomal markers LAMP1, LAMP2 and CD63. For all panels, HeLa cells were transfected with overexpression constructs for 48 h, fixed and immunostained as shown. Representative maximum intensity projections of serial confocal optical sections are shown. Nuclear DNA was visualised using DAPI. (b) The effects of ARL8B on signaling events downstream of mTORC1 are microtubule-dependent. HeLa cells were transfected either with ARL8B siRNA or with ARL8B overexpression construct for 48 h. In the final 5 h before harvest, cells were incubated without (DMSO), or with 1 μM nocodazole. Immunoblots with antibodies against phospho- and total-S6 protein and ARL8B are shown.

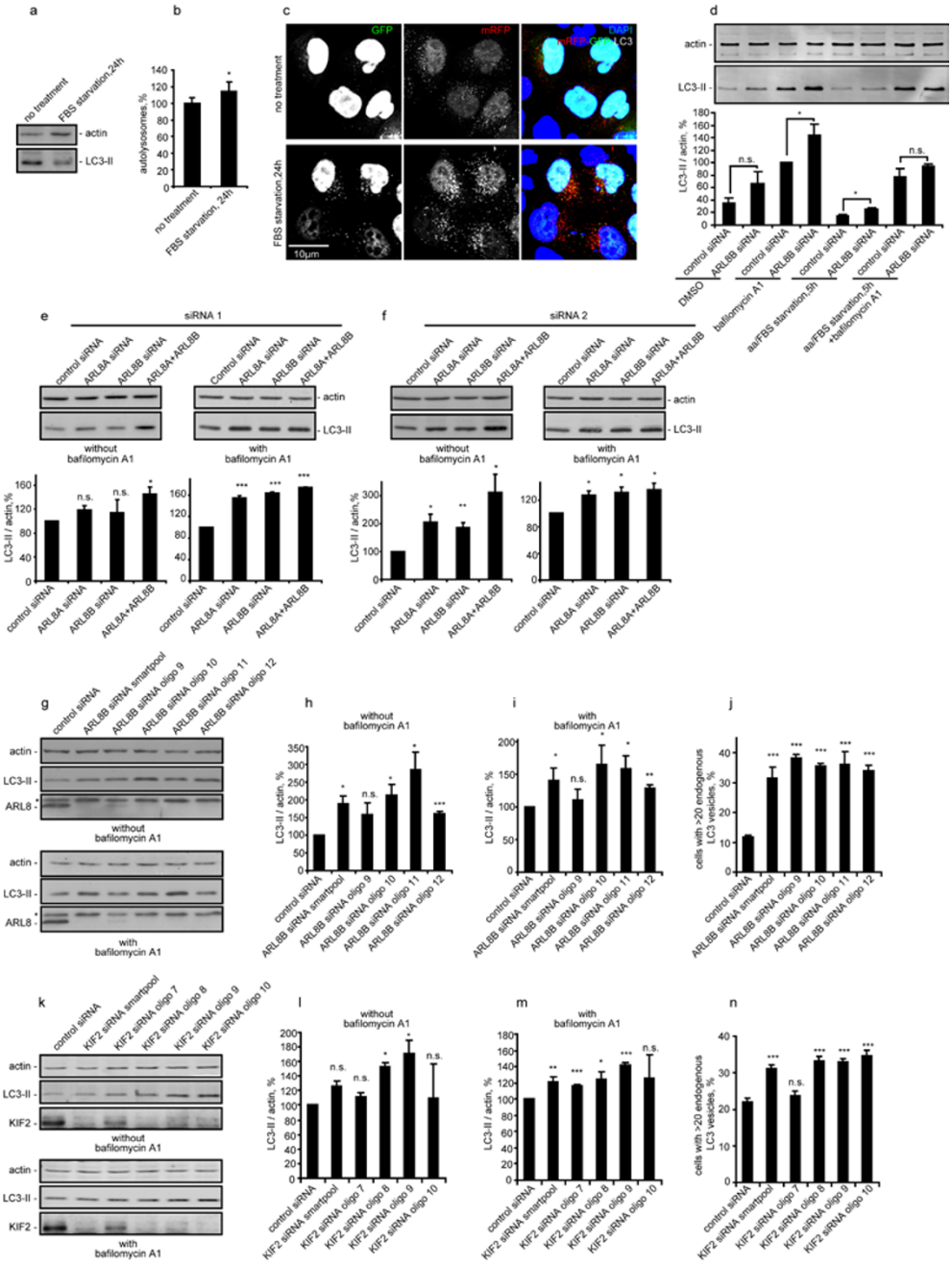

Figure S4 Effects of starvation, ARL8B and KIF2 on autophagy. (a-c) Serum starvation reduces levels of the autophagosomal marker LC3-II, but increases numbers of autolysosomes. (a) Control HeLa cells or cells deprived of serum for 24 h, were harvested and analyzed by immunoblotting. (b) HeLa cells stably expressing tfLC3 were treated as in (a), fixed and average numbers per cell of RFP-positive puncta (that lack GFP fluorescence) were quantified using automated microscopy. (c) Representative images of tfLC3-expressing HeLa used for automatic counting of autolysosome numbers as in (b). Representative maximum intensity projections of serial confocal optical sections are shown, GFP-positive vesicles represent autophagosomes, mRFP-only vesicles are autolysosomes. (d) Knockdown of ARL8B increases autophagosome synthesis in complete tissue culture medium but not in conditions of serum and amino acid starvation when mTOR activity is blocked. HeLa cells were transfected with control siRNA or siRNA against ARL8B for 72 h. Five hours before harvest cells were treated with or without bafilomycin A1 in complete tissue culture medium or in HBSS. Cells were immunoblotted and LC3-II levels relative to actin were quantified (bottom graph). (e) Knockdown of ARL8s increases synthesis of LC3-II. HeLa cells were transfected with control siRNA or siRNA against ARL8 proteins for 72 h with or without bafilomycin A1 treatment as in (d). Levels of LC3-II and actin were analyzed by immunoblotting (upper panels) and densitometry analysis relative to actin (lower graphs). (f) ARL8 knockdown using an alternative set of siRNA increases LC3-II levels. This is an experiment similar to that shown in (e) but uses an alternative set of siRNA (obtained from Invitrogen, see Methods) that target different regions of ARL8 mRNA compared our standard set of siRNA (Dharmacon). Levels of LC3-II and actin were analyzed by immunoblotting (upper panels) and densitometry analysis relative to actin (lower graphs). (g-j) Deconvolution of ARL8B siRNA smartpool demonstrates specificity of ARL8B siRNA effects on autophagosome synthesis. HeLa cells were transfected with individual siRNA oligonucleotides and treated as in (d). Asterisks indicate non-specific band. (h) and (i) Levels of LC3-II relative to actin were quantified. (j) Endogenous LC3-positive vesicles in siRNA transfected cells were visualised by immunofluorescence and the percentage of cells containing >20 vesicles per cell scored. (k-n) Deconvolution of KIF2 siRNA smartpool as in (g-j) for ARL8B.

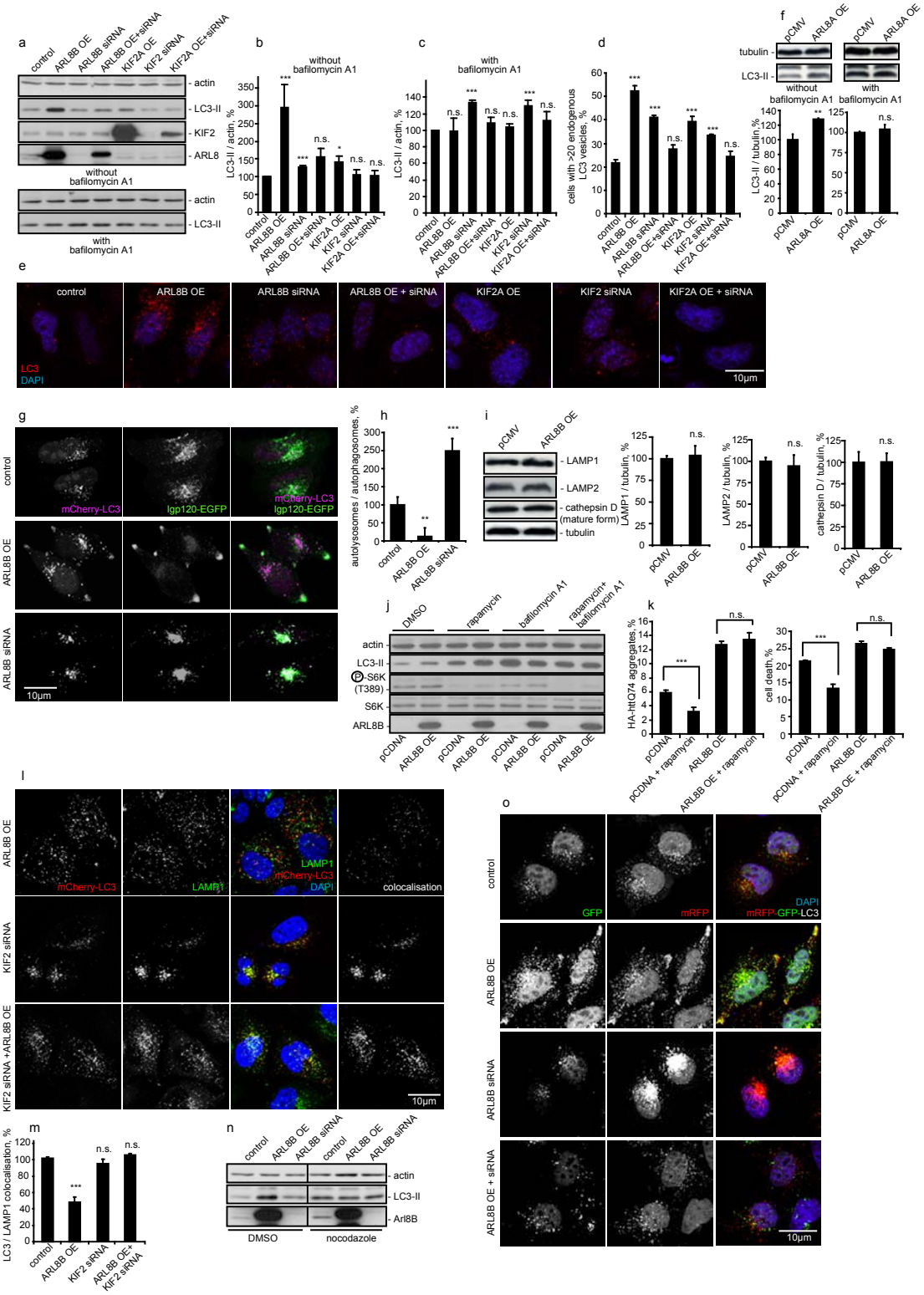

Figure S5 Effects of ARL8 and KIF2 on autophagy. (a-c) Overexpression and knockdown of ARL8B or KIF2 cancel the effect of each other on autophagosome synthesis. HeLa cells were transfected with smartpool siRNA against ARL8B or KIF2 (non-targeting SMARTpool siRNA was used as a control) with or without respective overexpression constructs for 48 h. Five hours before harvest cells were treated with or without 400 nM bafilomycin A1. Levels of LC3-II were analyzed by immunoblotting (a) and densitometry analyses relative to actin (b) and (c). (d) and (e) Simultaneous overexpression and knockdown of either ARL8B or KIF2 cancels their effect on the numbers of endogenous LC3 vesicles in HeLa cells. Panel (e) shows representative maximum intensity projections of serial confocal optical sections of cells transfected as in (a-c) and immunolabelled with anti-LC3 antibody (DAPI is used to visualise nuclei). (f) Overexpression of ARL8A inhibits degradation of LC3-II. HeLa cells were transfected with either control or ARL8A overexpression constructs for 48 h. In the final 16 h, cells were treated either with 200 nM bafilomycin A1 (with bafilomycin A1) or vehicle (DMSO, without bafilomycin A1). Levels of LC3-II and tubulin were analyzed by immunoblotting (upper panels) and densitometry analysis relative to tubulin (lower graphs) is shown. (g, h) HeLa cells were transfected with pCMV, ARL8B overexpression construct, or ARL8B siRNA, along with mCherry-LC3 and lgp120-EGFP for 48 h. Representative maximum intensity projections of serial confocal optical sections are shown in (g) and quantification of ARL8B effect on autophagosome-lysosome fusion is shown in (h). The percentages of autophagolysosomes (positive for both mCherry-LC3 and lgp120-EGFP) to all autophagosomes (positive for mCherry-LC3 and either positive or negative for lgp120-EGFP) were analysed with ImageJ. (i) HeLa cells were transfected with ARL8B overexpression construct or pCMV as a transfection control. Endogenous LAMP1, LAMP2, cathepsin D and tubulin were analysed by immunoblotting and densitometry analysis. (j) ARL8B overexpression inhibits autophagy by blocking autophagosome-lysosome fusion, even in conditions when its effect on mTOR signaling and autophagosome synthesis is rescued by rapamycin. HeLa cells overexpressing ARL8B or an empty vector as a control, were treated with DMSO (vehicle), rapamycin, bafilomycin A1 or both for 16 h before immunoblotting analysis. (k) ARL8B overexpression prevents rapamycin from inducing the clearance of an autophagy substrate. HeLa cells were transfected with pCDNA or ARL8B overexpression construct together with EGFP-httQ74. After 24 h cells, were further incubated with or without rapamycin during the last 24 h before fixation. The percentages of EGFP-positive cells with EGFP-httQ74 aggregates and with apoptotic nuclear morphology were quantified. (l) HeLa cells were cotransfected with ARL8B overexpression construct, KIF2A siRNA or both (and non-targeting siRNA and empty pEGFP vector were used as transfection controls) together with mCherry-LC3 for 48 h. After fixation, cells were stained for endogenous LAMP1 and DNA (DAPI). Representative maximum intensity projections of serial confocal optical sections are shown. Colocalisation panels show an overlap between mCherry-LC3 and LAMP1 signals. Note that the same set of images for ARL8B overexpression as in Fig. 5f of the main text is used here to facilitate the comparison. (m) Quantification of autophagosome-lysosome fusion. The percentages of autolysosomes (positive for both mCherry-LC3 and LAMP1) to autophagosomes (positive for mCherry-LC3 and negative for LAMP1) were quantified. (n) Effect of ARL8B on autophagy is microtubule-dependent. HeLa cells were transfected either with ARL8B siRNA or with ARL8B overexpression construct for 48 h with the last 5 h before harvest cells being incubated without (DMSO) or with 1 μM nocodazole. Immunoblots with antibodies against LC3, actin and ARL8B are shown. (o) Images of stably-expressing tfLC3 HeLa cells transfected with ARL8B overexpression plasmid, ARL8B siRNA or both. Representative maximum intensity projections of serial confocal optical sections are shown.

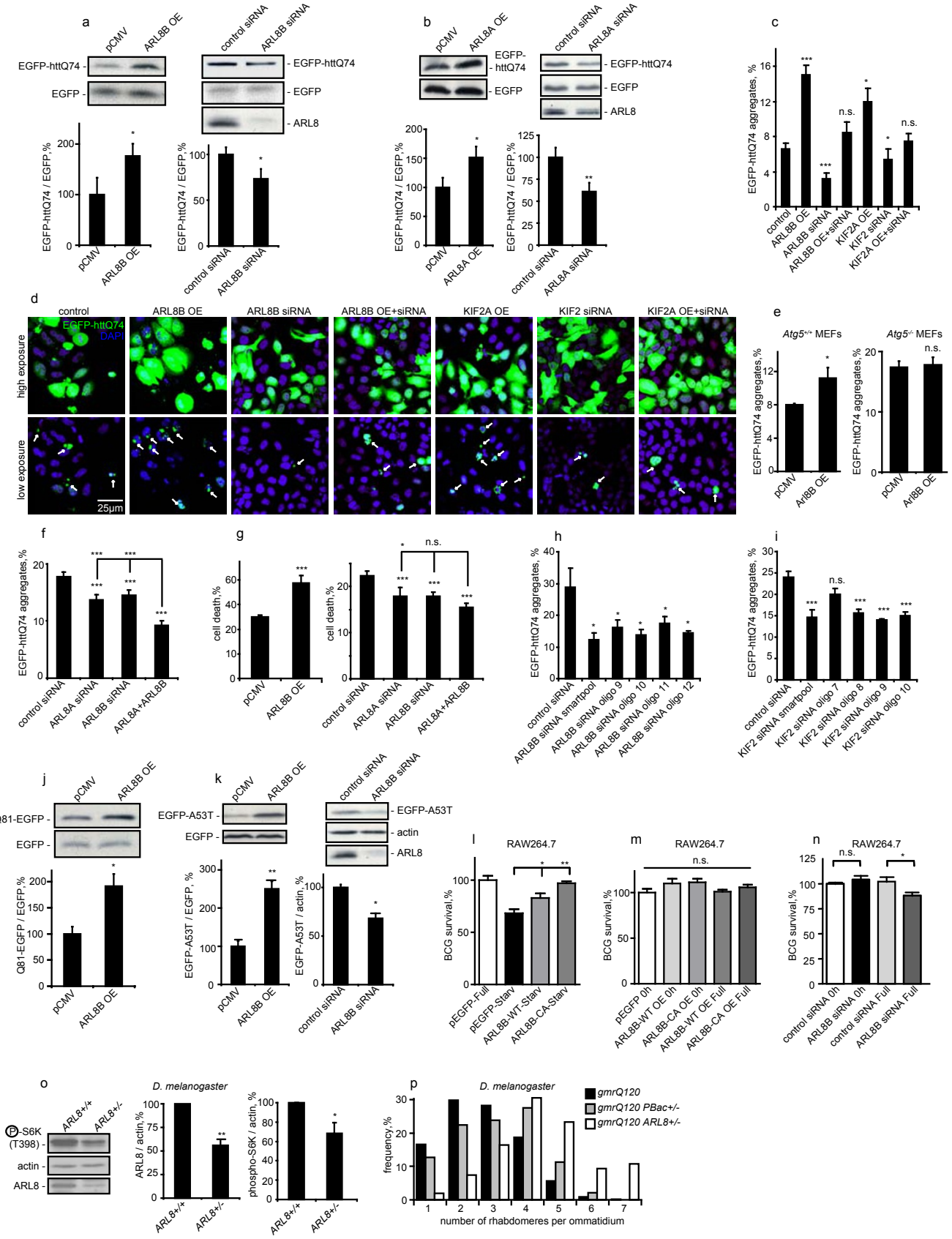

Figure S6 ARL8 and KIF2A proteins modulate degradation of clinically-relevant autophagic substrates. (a, b) ARL8B and ARL8A affect soluble levels of EGFP-tagged mutant huntingtin exon 1 (EGFP-httQ74). This models the Huntington's disease polyglutamine-expanded mutant protein, whose clearance is highly dependent on autophagy [21]. HeLa cells were cotransfected with ARL8 siRNA or overexpression constructs together with EGFP-httQ74 and pEGFP-C1 (transfection control) for 48 h. Cells were analyzed by immunoblotting with antibodies against EGFP and ARL8 (this antibody recognises both ARL8B and ARL8A proteins [12]) and densitometry analysis of soluble EGFP-httQ74 relative to EGFP (lower graphs). (c) and (d) Effect of ARL8B and KIF2 on formation of EGFP-httQ74 aggregates. HeLa cells were transfected with ARL8B or KIF2 overexpression constructs with or without siRNA against the same proteins together with EGFP-httQ74 for 48 h. Percentage of cells with EGFP-positive aggreagates is shown in (c). Representative confocal images of HeLa cells are shown in (d); arrows indicate intracellular aggregates of EGFP-httQ74. The result is in agreement with the fact that the percentage of cells with aggregates correlates with expression levels of these mutant huntingtin constructs [5]. (e) The effects of ARL8B on clearance of EGFP-httQ74 are mediated by autophagy. Wild-type (*Atg5*$^{+/+}$) or autophagy-deficient cells lacking the key autophagy gene *Atg5* (*Atg5*$^{-/-}$) mouse embryonic fibroblasts (MEFs) were cotransfected with EGFP-httQ74 and control or ARL8B overexpression constructs for 48 h. The percentages of EGFP-positive cells with EGFP-httQ74 aggregates were assessed. Since ARL8B overexpression increased the proportion of EGFP-httQ74 aggregates only in wild-type MEFs, but had no effect in autophagy-deficient cells, these ARL8B effects are autophagy-dependent. (f) and (g) Simultaneous knockdown of ARL8B and ARL8A has an additive effect on the percentages of cells with httQ74 aggregates. Also, consistently with toxicity of the polyglutamine constructs being a function of its levels, the percentage of EGFP-positive cells with EGFP-httQ74 aggregates and apoptotic nuclear morphology were increased by ARL8B overexpression and reduced by ARL8 knockdown (g). (h) and (i) Deconvolution of ARL8B and KIF2 siRNA smartpools demonstrates specificity of ARL8B and KIF2 siRNA effects on the formation of EGFP-httQ74 aggregates. HeLa cells were transfected with individual siRNA oligonucleotides together with EGFP-httQ74 for 48 h. The percentages of EGFP-positive cells with EGFP-httQ74 aggregates were quantified. (j) Overexpression of ARL8B increases the levels of an isolated polyglutamine expansion tagged onto EGFP (Q81-EGFP) [3]. HeLa cells were cotransfected with pCMV, ARL8B-Flag with EGFP-Q81 and pEGFP-C1 (transfection control) for 48 h. Soluble EGFP-Q81 and EGFP were analyzed by immunoblotting with antibody against EGFP (upper panels) and densitometry analysis relative to EGFP (lower graphs). Like huntingtin exon 1, these isolated polyglutamine tracts are aggregate-prone and are autophagy substrates [3]. (k) ARL8B inhibits autophagic degradation of A53T α-synuclein mutant. This mutant protein causes autosomal dominant forms of Parkinson's disease and is also highly dependent on autophagy for its clearance [22]. EGFP-A53T expression was induced in a stable HeLa cell line with doxycycline and cells were simultaneously transfected either with control or ARL8B siRNA, or with ARL8B and EGFP (transfection control) overexpression constructs for 48 h. EGFP-A53T expression was then switched off (by removing doxycycline) for 24 h, to allow us to determine effects on A53T turnover. Cells were collected and analysed by immunoblotting with antibodies against actin, EGFP and ARL8B and densitometry analysis relative to actin or EGFP (bottom graphs). (l) Overexpression of either wild type (ARL8B-WT) or constitutively active (ARL8B-CA) forms of ARL8B rescued BCG from autophagic elimination in starved macrophages. BCG is a mycobacterium related to the bacterium that causes tuberculosis and its clearance and survival in macrophage cell lines is modulated by autophagy [23, 24]. RAW264.7 macrophages transfected with pEGFP-C1, ARL8B-WT or ARL8B-CA for 24 h were infected with BCG for 1 h and incubated in starvation media for 2 h to examine the effect of ARL8B on starvation-induced, autophagic elimination of mycobacteria. (m) The effects of ARL8B on BCG elimination as seen in (l) are independent of either mycobacterial uptake or non-autophagic phagosomal biogenesis. RAW264.7 macrophages transfected with pEGFP-C1, ARL8B-WT or ARL8B-CA for 24 h were infected with BCG for 1 h and either lysed or incubated in DMEM (Full) for 2 h to examine the effect of ARL8B on mycobacterial uptake or normal intracellular survival. Neither process was significantly altered by overexpression of ARL8B. (n) ARL8B depletion enhanced the killing of BCG. RAW264.7 macrophages transfected with control siRNA or ARL8B siRNA for 24 h were infected with BCG for 1 h and incubated in DMEM. The cells were lysed to quantify bacterial survival by counting colony-forming units. No differences in mycobacterial uptake were observed after ARL8B siRNA-mediated depletion. (o) and (p) ARL8 knockdown protects against polyglutamine toxicity *in vivo* using a *Drosophila* model of HD. (o) Immunoblots of lysates (10 whole flies per group) from flies that carry *gmrQ120* in either a *w*^{1118} (*ARL8*$^{+/+}$) or an *ARL8* mutant heterozygous (*ARL8*$^{+/-}$) background. Levels of ARL8 and of phospho-S6K relative to actin in *ARL8*$^{+/-}$ flies compared to *ARL8*$^{+/+}$ flies were quantified and shown on graphs. (p) Mean numbers of rhabdomeres per ommatidium in 4-day old male flies. Flies heterozygous for the *ARL8 PBac[RB]* insertion (*gmrQ120 ARL8*$^{+/-}$) have significantly less neuronal degeneration ($p<0.01$ two-tailed paired t-test) as compared to either control line: *gmrQ120* in *w*^{1118} background (*gmrQ120 w*) or *gmrQ120* heterozygous for a control *PBac[RB]* insertion (*gmrQ120 PBac*$^{+/-}$). Data are based on 3 independent experiments, each with 300 ommatidia from 20 eyes. These data are consistent with the cell model data showing that ARL8 regulates polyglutamine toxicity.

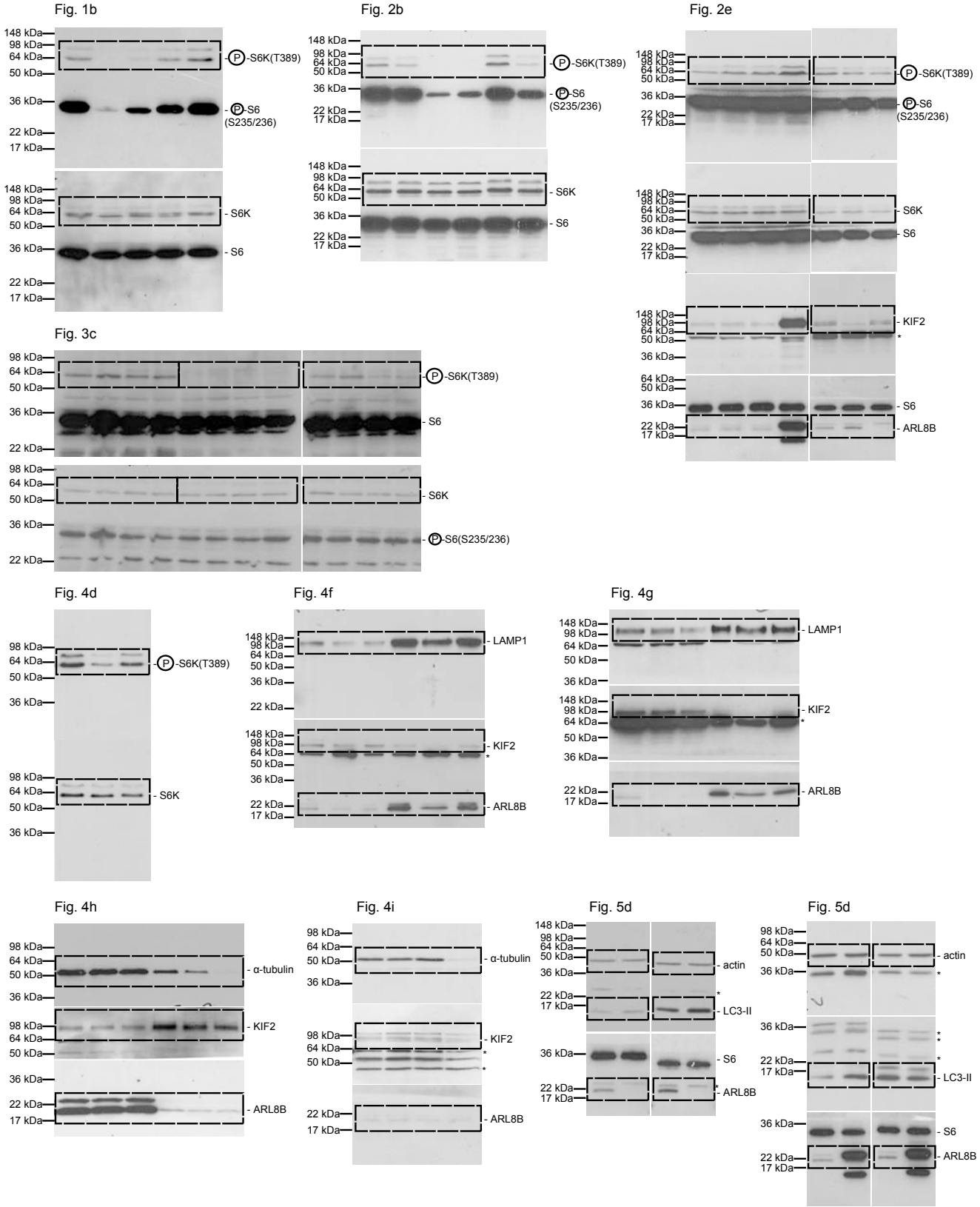

Figure S7 Full scans. Asterisks indicate non-specific bands.

References:

1. Kuma, A. *et al.* The role of autophagy during the early neonatal starvation period. *Nature* **432**, 1032-1036 (2004).
2. Noda, Y., Sato-Yoshitake, R., Kondo, S., Nangaku, M. & Hirokawa, N. KIF2 is a new microtubule-based anterograde motor that transports membranous organelles distinct from those carried by kinesin heavy chain or KIF3A/B. *J Cell Biol* **129**, 157-167 (1995).
3. Berger, Z. *et al.* Rapamycin alleviates toxicity of different aggregate-prone proteins. *Hum Mol Genet* **15**, 433-442 (2006).
4. Hofmann, I. & Munro, S. An N-terminally acetylated Arf-like GTPase is localised to lysosomes and affects their motility. *J Cell Sci* **119**, 1494-1503 (2006).
5. Narain, Y., Wyttenbach, A., Rankin, J., Furlong, R.A. & Rubinsztein, D.C. A molecular investigation of true dominance in Huntington's disease. *J Med Genet* **36**, 739-746 (1999).
6. Sarkar, S. *et al.* A rational mechanism for combination treatment of Huntington's disease using lithium and rapamycin. *Hum Mol Genet* **17**, 170-178 (2008).
7. Schlisio, S. *et al.* The kinesin KIF1Bbeta acts downstream from EglN3 to induce apoptosis and is a potential 1p36 tumor suppressor. *Genes Dev* **22**, 884-893 (2008).
8. Sarbassov, D.D. *et al.* Rictor, a novel binding partner of mTOR, defines a rapamycin-insensitive and raptor-independent pathway that regulates the cytoskeleton. *Curr Biol* **14**, 1296-1302 (2004).
9. Pryor, P.R., Reimann, F., Gribble, F.M. & Luzio, J.P. Mucolipin-1 is a lysosomal membrane protein required for intracellular lactosylceramide traffic. *Traffic* **7**, 1388-1398 (2006).
10. Zhou, X. *et al.* Rheb controls misfolded protein metabolism by inhibiting aggresome formation and autophagy. *Proc Natl Acad Sci U S A* **106**, 8923-8928 (2009).
11. Kimura, S., Noda, T. & Yoshimori, T. Dissection of the autophagosome maturation process by a novel reporter protein, tandem fluorescent-tagged LC3. *Autophagy* **3**, 452-460 (2007).
12. Okai, T. *et al.* Novel small GTPase subfamily capable of associating with tubulin is required for chromosome segregation. *J Cell Sci* **117**, 4705-4715 (2004).
13. Tafani, M. *et al.* Regulation of intracellular pH mediates Bax activation in HeLa cells treated with staurosporine or tumor necrosis factor-alpha. *J Biol Chem* **277**, 49569-49576 (2002).
14. Ong, V. *et al.* A role for altered microtubule polymer levels in vincristine resistance of childhood acute lymphoblastic leukemia xenografts. *J Pharmacol Exp Ther* **324**, 434-442 (2008).
15. Sarkar, S., Korolchuk, V., Renna, M., Winslow, A. & Rubinsztein, D.C. Methodological considerations for assessing autophagy modulators: a study with calcium phosphate precipitates. *Autophagy* **5**, 307-313 (2009).
16. Korolchuk, V.I., Mansilla, A., Menzies, F.M. & Rubinsztein, D.C. Autophagy inhibition compromises degradation of ubiquitin-proteasome pathway substrates. *Mol Cell* **33**, 517-527 (2009).
17. Ryder, E. *et al.* The DrosDel collection: a set of P-element insertions for generating custom chromosomal aberrations in Drosophila melanogaster. *Genetics* **167**, 797-813 (2004).
18. Thibault, S.T. *et al.* A complementary transposon tool kit for Drosophila melanogaster using P and piggyBac. *Nat Genet* **36**, 283-287 (2004).
19. Sancak, Y. *et al.* Ragulator-Rag complex targets mTORC1 to the lysosomal surface and is necessary for its activation by amino acids. *Cell* **141**, 290-303.
20. Sancak, Y. *et al.* The Rag GTPases bind raptor and mediate amino acid signaling to mTORC1. *Science* **320**, 1496-1501 (2008).
21. Ravikumar, B., Duden, R. & Rubinsztein, D.C. Aggregate-prone proteins with polyglutamine and polyalanine expansions are degraded by autophagy. *Hum Mol Genet* **11**, 1107-1117 (2002).
22. Webb, J.L., Ravikumar, B., Atkins, J., Skepper, J.N. & Rubinsztein, D.C. Alpha-Synuclein is degraded by both autophagy and the proteasome. *J Biol Chem* **278**, 25009-25013 (2003).
23. Gutierrez, M.G. *et al.* Autophagy is a defense mechanism inhibiting BCG and Mycobacterium tuberculosis survival in infected macrophages. *Cell* **119**, 753-766 (2004).
24. Singh, S.B., Davis, A.S., Taylor, G.A. & Deretic, V. Human IRGM induces autophagy to eliminate intracellular mycobacteria. *Science* **313**, 1438-1441 (2006).